MANIPULATION STRATEGIES FOR MASSIVE SPACE PAYLOADS

Semiannual Progress Report
May 15, 1991 - November 14, 1991

Wayne J. Book
Principal Investigator

The George W. Woodruff School
of Mechanical Engineering
Georgia Institute of Technology
Atlanta, GA 30332

NASA Grant NAG 1-623
(E25-517)

Technical Officer: Donald Soloway

SUMMARY

Graduate students supported during the reporting period included Doug Girvin, completing an M.S. Thesis, David Magee, an M.S. student planning to stay for a Ph.D., Jae Lew, a Ph.D. Student, and Soo-Han Lee a Ph.D. student nearing completion of his thesis.

Work during this period was continued with some difficulty, since the funding was slow to arrive at Georgia Tech.

Following the individual accounts of each of the student's work, a copy of publications (except theses) appears. Theses are submitted as separate reports.

Research Topic: Numerical Analysis of Nonminimum Phase Zeros

Research Assistant: Doug Girvin

Short Term Objective: Develop relationship between zero location and structural link design

Period Supported on Grant: June 1991-March 1992

This research targets nonminimum phase zero location of a single-link flexible manipulator. When the control objective is to accurately position the tip while the robot is actuated at the base, the system is nonminimum phase. One important characteristic of nonminimum phase systems are system zeros in the right half of the Laplace plane. Little research has been devoted to nonminimum phase zeros, but research in this area is necessary to better understand control of flexible manipulators. The ability to pick the location of these nonminimum phase zeros would give the designer a new freedom similar to pole placement.

First, a FORTRAN program was developed to determine the location of system zeros and poles given the model of the link. The program implements transfer matrix theory which allows the user to analyze links with nonuniform cross-sections. Second, the program was used to develop a relationship between structural link design and nonminimum phase zero location. A design method was developed for tapered links which allows the user to chose the first pole and zero location (subject to constraints), and to independently change the links mass moment of inertia about its axis of rotation. These choices will uniquely define the tapered link. Third, the results were used to generate the necessary data for implementing a tapered link design in a inverse dynamic control algorithm developed by a former research assistant. Fourth, the research was organized and presented in my Masters thesis this quarter. Currently I am working on organizing this research for a conference paper at the ASME Winter Annual Meeting this November.

Publications:

Girvin, Douglas L. and Wayne J.Book, "Numerical Analysis of Nonminimum Phase Zeros for Nonuniform Link Design," To appear in the proceedings of the ASME Symposium on "Dynamics of Flexible Multibody Systems: Theory and Experiment," ASME Winter Annual Meeting, Annaheim, CA, Nov. 8-13, 1992.

Research Topic: Robust Control of a Rigid Robot Carried by a Flexible Robot

Research Assistant: Soo-Han Lee

Short Term Objective: Complete Experimental Test of Theory

Period Supported on Grant: June 1991- December, 1991

When a small manipulator is carried by a large flexible manipulator, the inertial forces coupling the two systems can be used to damp vibrations. Control algorithms to do this have been reported in previous occasions. In this period it is our objective to experimentally verify their effectiveness.

Much effort has been required to produce a reliable experiment and to actually carry out the experiments.

Following the experiments the thesis writing will be completed.

Research Topic: Control of a Flexible Bracing Manipulator

Research Assistant: Jae Young Lew

Short Term Objective: Dynamics of Two Manipulators Serially Connected

Period Supported on Grant: September 91 - December 91

The concept of bracing strategy has been proposed to ensure accurate positioning of end effector and to support the force at the end effector due to the change in structural stiffness. This concept is applied to micro/macro manipulators which consist of a small arm mounted on the end of a large arm. This configuration allows a large robot to carry the small manipulator to the area of the interest. Then, the tip of the large arm braces against a stationary frame and use the small manipulator for fine motion control necessary to eliminate positioning error.

Short term objective is to obtain a closed form of the equations of motion for serially connected large and small manipulators. However, deriving the dynamic equations of these system can be a time consuming and recursive procedure. A simple method has been developed using the information from independently known dynamics of two manipulators. The proposed work identifies coupling dynamics between two arms instead of computing whole two arms' dynamics. This approach will reduce the number of computations significantly and show the structure of coupling dynamics between two arms.

The described method has been coded in *Mathematica* for symbolic computations. As a case study, the proposed technique is applied to two examples; *two links flexible arm with two links rigid arm* and *a moving vehicle with three links arm.* Each case shows at least one third computation time compared to the conventional derivation. Its publication is being prepared.

Research Topic: Reduction of Residual Vibration in a Flexible Manipulator

Research Assistant: David P. Magee

Short-Term Objective: Implement a modified command shaping technique to a teleoperated robot

Period Supported on Grant: June-December, 1991

The residual vibration of a flexible manipulator can be detrimental to the end-point positioning capabilities of the operator. To eliminate the vibration, a modified shaping technique was developed from previous work involving input shaping of command signals. The original input shaping method, developed by Seering and Singer, was studied and the robustness of the method investigated. To better evaluate the input shaping method, a different residual vibration equation was derived that better represents the technique. It was found that the input shaping method can actually increase the residual vibration if the system parameters are not accurately specified. In experiments with a 2-DOF, flexible manipulator, the input shaping method was shown to induce vibration in systems that have time-varying parameters, e.g. ω_n, ζ. To eliminate this vibration, a modified command shaping technique was developed. The new technique takes into account significant changes in system parameters and modifies the input shaping technique so that no vibration occurs. To test the modified method, sinusoidal perturbations at various frequencies were added to tip trajectories to simulate possible user inputs. By comparing frequency response data from an accelerometer mounted at the tip of a 2-DOF manipulator, the modified technique eliminated the unwanted residual vibration and yet preserved the usefulness of the commanded motion.

Publications:

1. Magee, D.P., *Dynamic Control Modification Techniques in Teleoperation of a Flexible Manipulator*," Master's Thesis, Georgia Institute of Technology, December, 1991.
2. Book, W.J. and Magee, D.P., "The Application of Input Shaping to a System with Varying Parameters," to appear in Japan-U.S.A. Symposium on Flexible Automation, July, 1992.
3. Book, W.J. and Magee, D.P., "Experimental Verification of Modified Command Shaping Using a Flexible Manipulator," to appear in Motion and Vibration Control, September, 1992.

PUBLICATIONS

1. Girvin, Douglas L. and Wayne J.Book, "Numerical Analysis of Nonminimum Phase Zeros for Nonuniform Link Design," To appear in the proceedings of the ASME Symposium on "Dynamics of Flexible Multibody Systems: Theory and Experiment," ASME Winter Annual Meeting, Annaheim, CA, Nov. 8-13, 1992.
2. Book, W.J. and Magee, D.P., "The Application of Input Shaping to a System with Varying Parameters," to appear in Japan-U.S.A. Symposium on Flexible Automation, July, 1992.
3. Book, W.J. and Magee, D.P., "Experimental Verification of Modified Command Shaping Using a Flexible Manipulator," to appear in Motion and Vibration Control, September, 1992.

Numerical Analysis of Nonminimum Phase Zero for Nonuniform Link Design

Douglas L. Girvin and Wayne J. Book

George W. Woodruff School of Mechanical Engineering
Georgia Institute of Technology
Atlanta, GA 30332

ABSTRACT

As the demand for light-weight robots that can operate in a large workspace increases, the structural flexibility of the links becomes more of an issue in control . When the objective is to accurately position the tip while the robot is actuated at the base, the system is nonminimum phase. One important characteristic of nonminimum phase systems is system zeros in the right half of the Laplace plane. The ability to pick the location of these nonminimum phase zeros would give the designer a new freedom similar to pole placement.

This research targets a single-link manipulator operating in the horizontal plane and modeled as a Euler-Bernoulli beam with pinned-free end conditions. Using transfer matrix theory, one can consider link designs that have variable cross-sections along the length of the beam. A FORTRAN program was developed to determine the location of poles and zeros given the system model. The program was used to confirm previous research on nonminimum phase systems, and develop a relationship for designing linearly tapered links. The method allows the designer to choose the location of the first pole and zero and then defines the appropriate taper to match the desired locations. With the pole and zero location fixed, the designer can independently change the link's moment of inertia about its axis of rotation by adjusting the height of the beam. These results can be applied to inverse dynamic algorithms currently under development at Georgia Tech and elsewhere.

INTRODUCTION

Controller design for collocated systems has been heavily researched and is well understood compared to controller design for noncollocated systems. In noncollocated systems, uncertainties from model inaccuracies and modal truncation present fundamental problems with system performance and stability [18]. The fundamental difference between collocated and noncollocated systems is the presence of these RHP zeros. To advance controller design for noncollocated systems, research needs to be conducted into the factors that affect the location of these RHP zeros. This research targets the relationship between RHP zeros and structural design.

Although research on RHP zeros is limited, there has been some notable research done in the past. In 1988, Nebot and Brubaker [13] experimented with a single-link flexible manipulator. In 1989, Spector and Flashner [19] investigated the sensitivity effects of structural models for noncollocated control systems. In 1990, Spector and Flashner [18] again studied modeling and design implications pertinent to noncollocated control. Also in 1990, Park and Asada [15],[14] investigated a minimum phase flexible arm with a torque actuation mechanism. In 1991, Park, Asada, and Rai [1] expanded their previous work on a minimum phase flexible arm with a torque transmission device.

The underlying issue in noncollocated control is how to deal with the RHP zeros in the control algorithm. A major step in solving the problem is understanding what design parameters can be used to change the location of these RHP zeros. This research targets the relationship between RHP zero location and structural design. Specifically, how do changes in the shape of the structure (link) affect the location of these zeros?

Traditionally links are designed with uniform properties along the length because analytic solutions to this problem exist. A link with variable cross-section cannot be solved analytically, but with aid of a computer a numerical approximation can be found. The key to an accurate numerical solution is a good model of the system.

The research presented in this paper models a single-link flexible rotary manipulator as a pinned-free beam. Transfer matrix theory was used to generate a beam with variable cross-section. FORTRAN code was written to generate the model and evaluate the system for the location of RHP zeros. The program was used to examine the relationship between link shape and RHP zero location. This

relationship can be directly applied to controller design using the inverse dynamics approach researched at Georgia Tech and elsewhere.

TRANSFER MATRIX THEORY

Transfer matrices describe the interaction between two serially connected elements. These elements can be beams, springs, rotary joints, or many others. In 1979 Book, Majette, and Ma [6] and Book [4] (1974) used transfer matrices to develop an analysis package for flexible manipulators. They used transfer matrices to serially connect different types of elements to model the desired manipulator. Of interest in this paper is how to connect similar types of transfer matrices (beam elements) to model a beam with different cross-sectional area. Pestel and Leckie [16] provide an in depth discussion of transfer matrix derivations and applications.

Transfer matrices can be mathematically expressed by Equation 3.1. The state vector u_i is given by the state vector u_{i-1} multiplied by the transfer matrix B.

$$u_i = [B_i]u_{i-1} \tag{3.1}$$

When elements are connected serially, the states at the interface of two elements must be equal. By ordered multiplication of the transfer matrices, intermediate states can be eliminated to determine the transfer matrix for the overall system.

The concept of state vector in transfer matrix theory is not to be confused with the state space form of modern control theory. The state equation in modern control theory relates the states of the system as a function of time. In transfer matrix theory the state equation relates the states at various points along the serial chain of elements. The independent variable in a transfer matrix is the Laplace or Fourier variable with units of frequency, not time. The elements of the matrix B depend on the frequency variable and therefore the states will change as the system frequency changes. The transfer matrix B essentially contains the (Laplace or Fourier) transformed dynamic equations of motion that govern the element in analytic form. Therefore, analytical solution of the transfer matrix alone does not involve numerical approximations to the partial differential equation modelling the beam. This is desirable since numerical approximations introduce error into the solution.

A single-link manipulator as pictured in Figure 3.1 can be thought of as a beam with torque applied at one end and free at the other end. There are several steps to determine the RHP zeros and imaginary poles of this system. First, develop a model for the beam. Second, determine the appropriate boundary conditions. Third, determine the system input and output. Fourth, solve for the system zeros. The following sections will discuss each of these steps in more detail.

A link with nonuniform cross-sections can be modeled as a series of discrete elements. While the shape of these elements is similar, the size can vary to allow for changes in cross-section. The appropriate element to model a flexible link is an Euler-Bernoulli beam element. The Euler-Bernoulli model neglects the effects of rotary inertia and shear deformation in the element. [11]. This assumption is generally valid for modeling beams whose length is roughly ten times the thickness. Flexible manipulators have long, slender links which are appropriately modeled under the Euler-Bernoulli assumption.

Transfer matrices are derived from the equation of motion for a given element. For a uniform Euler-Bernoulli beam element, the equation of motion transformed to the frequency domain has the form:

$$\frac{d^4w(x,\omega)}{dx^4} = \frac{\mu\omega^2}{EI}\, w(x,\omega)$$

where,

μ	=	mass density per unit length
ω	=	frequency in radians/second
E	=	Young's modulus
I	=	Cross sectional area moment of inertia

Notice the equation is fourth order thus requiring four states to describe the solution in transfer matrix form. The state vector for the Euler-Bernoulli element is:

$$u = \begin{bmatrix} -w \\ \psi \\ M \\ V \end{bmatrix} = \begin{bmatrix} displacement \\ slope \\ moment \\ shear\ force \end{bmatrix} \tag{3.3}$$

The first two elements of the state vector are displacements (w and ψ) while the last two elements are forces (V and M). This arrangement of states is characteristic of transfer matrix theory.

An analytic solution to Equation 3.2 can be found when the element has uniform properties (ie. constant cross-section, mass density, and stiffness). Equation 3.4 gives the transfer matrix for a uniform Euler-Bernoulli element. Each element of Equation 3.4 is a function of frequency and must be reevaluated as the frequency of interest changes.

$$TM = \begin{bmatrix} C_0 & lC_1 & aC_2 & alC_3 \\ \frac{\beta^4 C_3}{l} & C_0 & \frac{aC_1}{l} & aC_2 \\ \frac{\beta^4 C_2}{a} & \frac{\beta^4 lC_3}{a} & C_0 & lC_1 \\ \frac{\beta^4 C_1}{al} & \frac{\beta^4 C_2}{a} & \frac{\beta^4 C_3}{l} & C_0 \end{bmatrix} \tag{3.4}$$

where,

$$C_0 = \frac{1}{2}(\cosh\beta + \cos\beta) \quad (3.5)$$

$$C_1 = \frac{1}{2\beta}(\sinh\beta + \sin\beta) \quad (3.6)$$

$$C_2 = \frac{1}{2\beta^2}(\cosh\beta - \cos\beta) \quad (3.7)$$

$$C_3 = \frac{1}{2\beta^3}(\sinh\beta - \sin\beta) \quad (3.8)$$

and

$$\beta^4 = \frac{\omega^2 l^4 \mu}{EI} \quad (3.9) \qquad a = \frac{l^2}{EI} \quad (3.10)$$

With the transfer matrix for the fundamental beam elements, one can combine these elements serially to generate a model for the link. Figure 3.3 illustrates how a simple model can be constructed for a tapered beam. Although only two elements are considered here, more elements can be added to better approximate the shape of the link. Since the states at interface u_1 are the same for both elements, u_1 can be eliminated to obtain an overall transfer matrix for the beam:

$$u_2 = [B_2][B_1]u_0 \quad (3.13)$$

Eliminating one state simply illustrates the point that this multiplication can be carried out to eliminate all intermediate states in a model with more elements.

As previously mentioned, transfer matrices themselves are not numerical approximations. The transfer matrix for a Euler-Bernoulli beam contains the analytic solution for a uniform beam element. It is not an assumed modes solution. The approximation made in using transfer matrix theory involves the modeling of the beam and solution of the equations. To generate the model of a link with variable cross-section, the size of the elements must vary. The interface of two different size elements will be discontinuous. In Figure 3.3, interface 1 is discontinuous between elements A and B. These discontinuities are the major approximation when using transfer matrices to model a beam. This approximation can be minimized by using more elements to model a nonuniform beam. As more elements are added to the model, the discontinuities between elements will decrease thus reducing the effects of this approximation on the results.

Transfer matrix theory as used to represent a variable cross section is similar to Finite Element Analysis (FEA). In FEA, first the system must be discretized. Then an appropriate interpolation function must be selected to describe each element (ie. element stiffness). Next the system matrices must be assembled to produce a set of linear algebraic equations. Finally the linear equations are solved to get an approximate solution to the system under consideration. These boundary conditions are applied to the overall transfer matrix for the system and the appropriate state variables are set to zero.

$$\begin{bmatrix} -w \\ \psi \\ 0 \\ 0 \end{bmatrix}_{x=L} = \begin{bmatrix} B_{11} & \cdots & B_{14} \\ \vdots & \ddots & \vdots \\ B_{41} & \cdots & B_{44} \end{bmatrix} \begin{bmatrix} 0 \\ \psi \\ 0 \\ V \end{bmatrix}_{x=0} \quad (3.14)$$

Since this research targets the location of RHP zeros the system output is tip position, and the system input is joint torque. Considering the system input and output, the overall system transfer matrix will have the form:

$$\begin{bmatrix} -w \\ \psi \\ 0 \\ 0 \end{bmatrix}_{x=L} = \begin{bmatrix} B_{11} & \cdots & B_{14} \\ \vdots & \ddots & \vdots \\ B_{41} & \cdots & B_{44} \end{bmatrix} \begin{bmatrix} 0 \\ \psi \\ \tau \\ V \end{bmatrix}_{x=0} \quad (3.15)$$

In the above equation, w_L is the system output which corresponds to tip position, and τ is the system input corresponding to joint torque at the base of the manipulator.

With the system input and output chosen, Equation 3.15 can be simplified to relate system input to system output:

$$N = B_{12}B_{44}B_{33} - B_{12}B_{34}B_{43} + B_{13}B_{34}B_{42} - B_{13}B_{44}B_{32} + B_{14}B_{43}B_{32} - B_{14}B_{33}B_{42}$$

$$w_L = -\frac{N}{B_{34}B_{42} - B_{44}B_{32}} \quad (3.16)$$

Where B_{ij} are elements of the overall transfer matrix in Equation 3.15. When the frequency is found which renders the function inside the brackets zero the output at that frequency will always be zero regardless of the input; therefore, the zeros of the bracketed term are the system zeros.

To search for RHP zeros, one must consider what type of frequency to input into Equation (3.16). Using the relationship which defines the Laplace variable, s

$$s = j\omega \quad (3.17)$$

one can easily determine ω should have the form:

$$\omega = 0 - jb \qquad where \quad 0 \le b \le \infty \quad (3.18)$$

That is, imaginary negative values of ω will result in purely real positive values of s. Thus searching Equation 3.16 with frequencies of the form of Equation 3.17 one can find the location of the RHP zeros on the real axis.

Although the location of RHP zeros is of primary concern in this research, knowledge of pole location will help in analysis of the results. Since the system damping is ignored, the poles will lie on the imaginary axis of the s-plane in complex conjugate pairs. The location of these poles can be determined by simply searching the positive imaginary axis of the s-plane. Considering the applied boundary conditions, one can extract two homogeneous equations from Equation 3.14 to get the homogeneous system:

$$\begin{Bmatrix} 0 \\ 0 \end{Bmatrix} = \begin{bmatrix} B_{32} & B_{34} \\ B_{42} & B_{44} \end{bmatrix} \begin{Bmatrix} \psi \\ V \end{Bmatrix} \tag{3.19}$$

The poles (eigenvalues) of the system are those values of ω which make the determinant of the sub-transfer matrix in Equation 3.19 equal to zero (see reference [6] for a detailed explanation). For a two by two matrix this determinant is simply:

$$g(\omega) = B_{32}B_{44} - B_{34}B_{42} \tag{3.20}$$

Referring to Equation 3.17, one finds that Equation 3.20 is the denominator of the input/output transfer function which is to be expected. To find the values of the purely complex poles, one must search Equation 3.20 for its roots. According to the definition of s, ω must have the form:

$$\omega = b + j0 \tag{3.21}$$

Searching over a range of values for b will give the poles in that range. With the zero and natural frequency functions determined, the problem remains to implement a computer solution to find the RHP zeros and imaginary poles.

RESULTS

Unless otherwise specified, several dimensions remain the same from one study to the next (referred to as nominal dimensions). The overall length of the beams is 40 inches, and the height (which remains constant over length) is 1 inch. The material properties are selected to be those of aluminum: modulus of elasticity, E, is 10E6 psi, and the density is 9.55E-2 lbm/in^3.

Although the model was limited to uniform elements, there were any number of combinations one can find to represent the system. This study examined two different methods for modeling a linearly tapered beam. As shown in Figure 4.1 the link was tapered along the length in the width dimension while the height was held constant. The taper was described by two dimensions: the width at the base, A, and the width at the tip, B. The degree of taper, R=A/B, was used to compare different designs.

Using Method 1 to model the tapered link, the beam was divided into elements of equal length. For a three element model with length L, each element will have length L/3. The height of each element was the same, while the width of each element changed linearly as a function of x. Figure 4.2 presents modeling Method 1.

Using Method 2 to model the tapered link, the beam was divided into elements so the first and last element have length one-half of the intermediate elements. For a three element model with length L, the first and last elements will have length L/4 and the middle element will have length L/2. Again the height of each element was the same, while the width of each element changed linearly as a function of x. Figure 4.3 presents modeling Method 2.

Figures 4.2 and 4.3 illustrate the main difference between the two modeling methods. Method 2 compensated the elements at each end for meeting the specified end widths A and B. In both methods the width of intermediate elements was determined by the width of the tapered beam at the midpoint of each element. Since the end elements meet the specified A and B, the tapered link will not pass through the midpoint of these two elements. Method 2 compensates for this exception by making the end element lengths one half the length of the other elements.

To compare these two different modeling methods for a linearly tapered beam, a beam with nominal dimensions and A=0.75 inches and B=0.25 inches was studied. This corresponds to R=3. The number of elements was increased with each method until the zeros and poles converged. Table 4.3 presents the results from Method 1 where all elements were of equal length, and Table 4.4 presents the results from Method 2 where the end elements were half the length of all other elements. Although only two methods are considered in this research, there are many different ways to discretize a nonuniform link.

The two methods were evaluated based on an error function. When the tapered beam was modeled with 80 elements, both methods converged to nearly identical values for the poles and zeros. These values, when NE=80, were taken to be the "correct' values and other cases were compared to this case. The error, e, was defined for the zeros as:

$$e = \left| \frac{z_{80,i} - z_{NE,i}}{z_{80,i}} \right| \tag{4.2}$$

where i refers to the i^{th} zero

A similar definition was used for the poles. The value of e at the top of each column represents the maximum of all individual errors in each column. As the tables show, Method 2 provided better results for the same number of elements. In each table, one column was shaded to distinguish it as the number of elements needed to get the error under 1%. For Method 2, this column corresponded to NE=10 as opposed to NE=20 for Method 1. Thus, compensating the end elements did provide a better model of a linearly tapered beam, and this method was used in the following studies unless specified otherwise.

When comparing different link designs to evaluate pole/zero location as a function of link shape, it was

necessary to keep some parameter constant to aid in the evaluation. For a single-link manipulator rotating in the horizontal plane, the link's mass moment of inertia about its axis of rotation, I_y, was of importance. This parameter directly affected the dynamic equations of motion and was an important design parameter in terms of motor selection. In the following studies, several link designs were evaluated for a given value of I_y. A tapered link's moment of inertia about its axis of rotation in terms of the links parameters: L, A, B, H, and ρ is found to be:

$$I_y = \frac{\rho H}{48}(A^3 + A^2B + AB^2 + B^3 + 4AL^2 + 12BL^2) \tag{4.3}$$

For a given tapered link design, one can use Equation 4.3 to determine I_y. Knowing I_y, one can change the value of A and solve Equation 4.3 for B. Since the equation was cubic in B, the commercial package *Mathematica* was used to solve for B. Following this method, a group of tapered link designs were generated all with the same I_y.

The first study investigated several tapered link designs with nominal dimensions and all designs having I_y=764.05 in-lb-sec^2. Table 4.5 presents the raw data for each of these designs. Even with I_y held constant, it was still difficult to interpret the data. To aid in developing a relationship between zero location and link shape, the zeros were normalized with respect to the first pole for each design. The first pole is an important parameter in control system design, and normalizing the zeros with respect to the first pole aided in the interpretation of the results. Table 4.6 presents the normalized data for those designs with I_y=764.05 in-lb-sec^2. The second study presents data for several link designs with nominal dimensions and I_y=1528.1 in-lb-sec^2. Table 4.7 shows the raw data for these link designs and Table 4.8 shows the normalized data for these designs. Figures 4.4 and 4.5 show pole/zero maps for selected values of R for I_y=764.05 and I_y=1528.1 respectively.

Several patterns were evident by examining the raw data. First as a general rule, both the poles and zeros increased (moved away from the origin) as the taper on the beam increased. Increasing the taper effectively moved more of the link mass closer to the base. Increasing the value of the poles is often desirable to push them out of the system bandwidth and increase system response speed. The ordering of poles and zeros was the second pattern recognized. In a collocated system, the poles and zeros will both lie on the imaginary axis in complex conjugate pairs and in an alternating order. This means, along the imaginary axis, the poles and zero are found in the order p_1, z_1, p_2,z_2, etc. or vice versa. Previous research [18] has found this alternating order of poles and zeros does not hold for nonminimum phase systems. Referring to Table 4.5, notice the order of the magnitude of poles and zeros was: z_1,p_1,p_2,z_2,p_3,z_3,p_4,p_5,z_4.... p_2 jumped in front of z_2, and the same occurred for p_5. This reordering of poles and zeros can be critical as accurate knowledge of the pole/zero order is important for control system design.

Important information was learned from examining the relationship between the taper ratio, R, and the values of the normalized zeros. Figure 4.8 better illustrates this point showing both polynomial fits on the same graph. Even though the coefficients were different for each polynomial fit, the curves were nearly identical.

This illustrates an important relationship in the design of tapered links. For a given ratio R, the normalized zero will always remain the same. The designer can choose the location of the first pole and zero, determine the normalized zero, and then using Figure 4.8 find the appropriate taper ratio R. Of course there are constraints on this process. A ratio less than one corresponds to a taper with B greater than A, which is usually undesirable. At the other end, R is limited by the value of H. If A is larger than the value of H, the link will be wider at the base than it is tall, and the assumption that the link is stiff in the vertical plane will no longer be valid. Although the designer can choose the pole/zero relationship, the values of normalized zeros are limited to approximately 0.72-0.82 (according to Figure 4.8).

A simple verification of the above relationship is the uniform beam which has no taper. According to the stated relationship, the normalized first zero should be the same for all uniform beams. Table 4.9 presents the results for several uniform beam designs. All cases had nominal dimensions. The normalized zero in all cases was 0.726 which confirmed the normalized zero will not change as long as R is constant.

Previous studies demonstrated how the designer can choose the pole/zero relationship and then determine the appropriate taper design from the ZERO results. This study presents the designer with another freedom. Once the taper is chosen, the designer can change the link to independently adjust the value of I_y. Table 4.10 presents the results of a study performed on designs with L=40 inches, and all designs have the same taper. The height of the link was changed to adjust the value of I_y.

One should notice that the pole and zero locations of all designs in Table 4.10 were the same, yet the value of I_y changed with adjustments in link height. Since the adjustment of H is out of the plane of motion, it had no effect on the location of poles and zeros. Combining this with the results from the previous study, the designer can effectively choose the location of poles and zeros and independently adjust the links moment of inertia about its axis of rotation to meet the needs of the particular system.

CONCLUSIONS

Program ZERO was developed as a tool to locate the poles and zeros of a single-link manipulator modeled as a pinned-free Euler-Bernoulli beam. The program used transfer matrix theory to allow for variable cross-sections granting the designer new freedom in analysis of nonuniform link designs. The results were shown to be very accurate when system pole location was compared to analytic solutions for uniform beams. Several results from previous studies were confirmed with this research.

First, the reordering of poles and zeros was confirmed for nonminimum phase systems. Accurate knowledge of pole/zero order is critical for proper control system design. In conjunction with this, Tables 4.3 and 4.4 show that even for very few elements in the model, the program still predicts the proper order of poles and zeros.

Second, the studies presented suggested the nonminimum phase characteristics could not be eliminated by changing the structural design of the link. The system will be nonminimum phase above a finite frequency dictated by the location of the first nonminimum phase zero. It may be possible that this frequency is out of the operating range and not of concern to the designer.

The major contributions of this research are the development of the ZERO program to determine zero and pole location for a single-link nonuniform flexible manipulator, and formulation of a design procedure to place the first pole and zero and independently change the value of the link's moment of inertia about its axis of rotation to meet the needs of the system.

Program ZERO was set up specifically for pinned-free boundary conditions of the model and determines pole and zero location based on a frequency range entered by the user. Linearly tapered beams were studied in this research, but any type of nonuniform beam can be analyzed by program ZERO. Slight modifications would also allow for different boundary conditions.

The design procedure for tapered beams allows the designer to choose the first pole and zero subject to certain physical constraints. These physical constraints only allow for approximately 25% variation in R according to Table 4.6. This zero to pole ratio defines a particular taper ratio according to the collected data. Keeping the ratio the same, the size of the taper can be changed to get the proper magnitude of the pole and zero. With the pole and zero placed, the height of the beam can be changed to adjust the link's moment of inertia about its axis of rotation. This procedure can be used to design tapered links to meet the particular requirements of the system.

Program ZERO was designed to model a single-link manipulator modeled with pinned-free boundary conditions. This is a simplified model, but it was necessary to show transfer matrices yield good results for this case before progressing to more complicated problems. Now that transfer matrices have proven useful to solve for zero location, future work exists to extend the results of this research.

First, the program could be modified so the user could input the desired boundary conditions which best represent the system. This could include hub inertia or end-point mass. Second, the program could be extended to multi-link designs to predict pole and zero location for different configurations. Transfer matrices have been derived for rotary joints and many other elements. The DSAP package developed by Book, et. al. [6] handles multi-link models and would be a good reference. Finally, the results for tapered link designs could be applied to the inverse dynamic algorithm developed by Kwon and Book [9]. This method requires mode shapes for the assumed modes and uses pinned-pinned boundary conditions, which can also be found using transfer matrix techniques as shown in Book, et al.[6].

ACKNOWLEDGEMENTS

This work was performed with partial support from grant NAG 1-623 from the National Aeronautics and Space Administration. NASA bears no responsibility for its content.

BIBLIOGRAPHY

[1] Asada, H., Park, J.-H., and Rai, S., "A Control-Configured Flexible Arm: Integrated Structure/Control Design," *Proceedings of the 1991 IEEE International Conference on Robotics and Automation*, Sacramento, California, April, 1991, pp. 2356-2362.

[2] Bayo, E., "A Finite Element Approach to Control the End-Point Motion of a Single-Link Flexible Robot," *Journal of Robotic Systems*, Vol. 4, No. 1, 1987, pp.63-75.

[3] Beer, Ferdinand, and Johnson, Russell, Jr., *Vector Mechanics for Engineers, Statics and Dynamics*, Third Edition, McGraw-Hill, New York, 1977.

[4] Book, W. J., *Design and Control of Flexible Manipulator Arms*, Ph.D. Thesis, Massachusetts Institute of Technology, April, 1974.

[5] Book, W. J., and Kwon, D.-S., "Contact Control for Advanced Applications of Light Weight Arms," *Symposium on Control of Robots and Manufacturing*, Arlington, Texas, 1990.

[6] Book, W. J., Majette, M., and Ma, K., *The Distributed Systems Analysis Package (DSAP) and Its Application to Modeling Flexible Manipulators*, NASA Contract NAS 9-13809, Subcontract No. 551, School of Mechanical Engineering, Georgia Institute of Technology, 1979.

[7] Churchill, R. V., and Brown, J. W., *Complex Variables and Applications*, Fifth Edition, McGraw-Hill Publishing Company, New York, 1990.

[8] Kwon, D.-S., *An Inverse Dynamic Tracking Control for Bracing A Flexible Manipulator*, Ph.D. Dissertation, Georgia Tech, Woodruff School of Mechanical Engineering, June, 1991.

[9] Kwon, D.-S., and Book, W. J., "An Inverse Dynamics Method Yielding Flexible Manipulator State Trajectories," *Proceedings of the American Control Conference*, June, 1990, pp. 186-193.

[10] Majette, M., *Modal State Variable Control of a Linear Distributed Mechanical System Modeled with the Transfer Matrix Method*, Master's Thesis, Georgia Tech, Woodruff School of Mechanical Engineering, June, 1985.

[11] Meirovitch, L., *Elements of Vibrational Analysis*, McGraw-Hill, New York, 1986.

[12] Misra, Pradee, "On The Control of Non-Minimum Phase Systems," *Proceedings of the 1989 American Control Conference*, 1989, pp. 1295-1296.

[13] Nebot, E. M., Lee, G. K. F., and Brubaker, T. A., "Experiments on a Single Link Flexible Manipulator,", *Proceedings from the USA-Japan Symposium on Flexible Automation Crossing Bridges: Advances in Flexible Automation and Rob[illegible]s*, 1988, pp. 391-398.

[14] Park, J.-H., and Asada, H., "Design and Analysis of Flexible Arms for Minimum-Phase Endpoint Control," *Proceedings of the American Control Conference*, 1990, pp. 1220-1225.

[15] Park, J.-H., and Asada, H., "Design and Control of Minimum-Phase Flexible Arms with Torque Transmission Mechanisms," *Proceedings of the 1990 IEEE International Conference on Robotics and Automation*, 1990, pp. 1790-1795.

[16] Pestel and Leckie, *Matrix Methods in Elastomechanics*, McGraw-Hill, New York, 1963.

[17] Rao, Singiresu S., *Mechanical Vibrations*, Addison-Wesley Publishing Company, Reading, Massachusetts, 1986.

[18] Spector, V. A., and Flashner, H., "Modeling and Design Implications of Noncollocated Control in Flexible Systems," *Journal of Dynamic Systems, Measurement, and Control*, Vol. 112, June, 1990, pp. 186-193.

[19] Spector, V. A., and Flashner, H., "Sensitivity of Structural Models for Noncollocated Control Systems," *Journal of Dynamic Systems, Measurement, and Control*, Vol. 111, December, 1989, pp. 646-655.

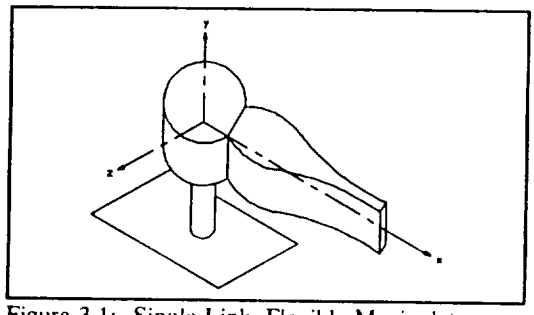

Figure 3.1: Single-Link, Flexible Manipulator

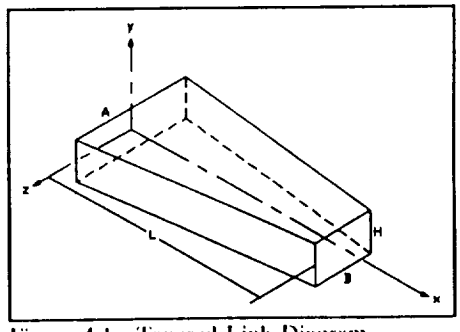

Figure 4.1: Tapered Link Diagram

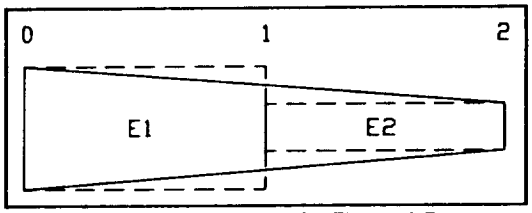

Figure 3.3: Simple Model of a Tapered Beam

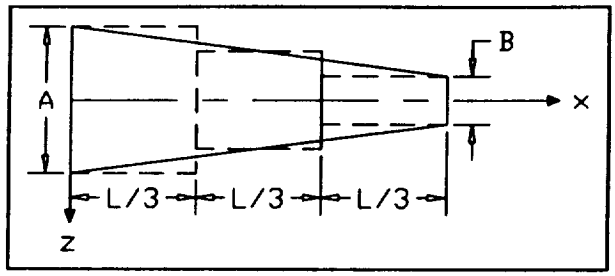

Figure 4.2: Modeling Method 1

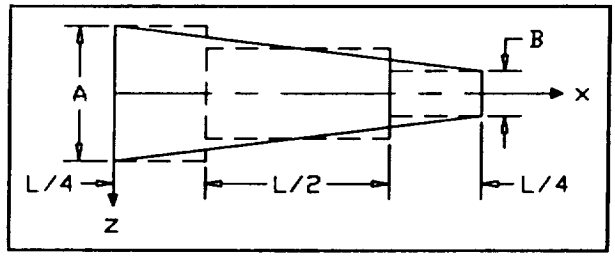

Figure 4.3: Modeling Method 2

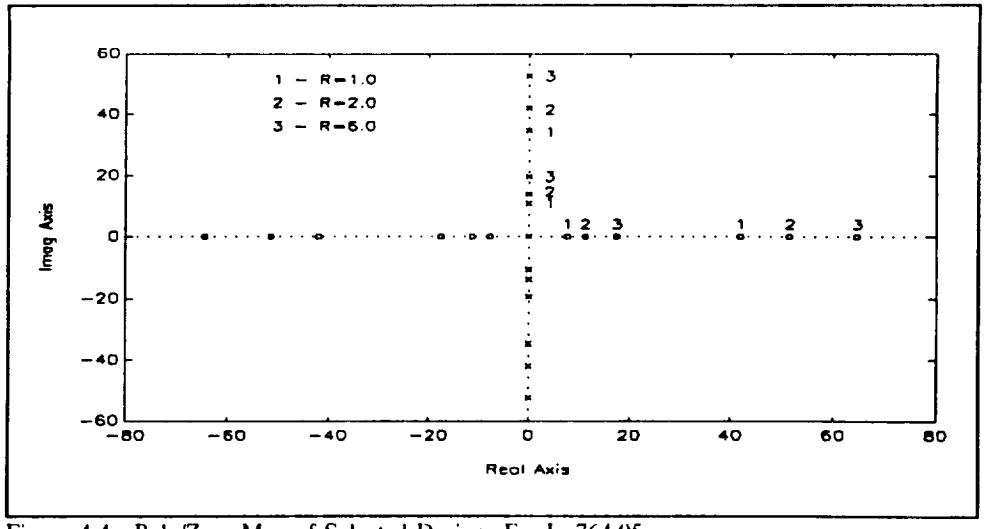

Figure 4.4: Pole/Zero Map of Selected Designs For I_y=764.05

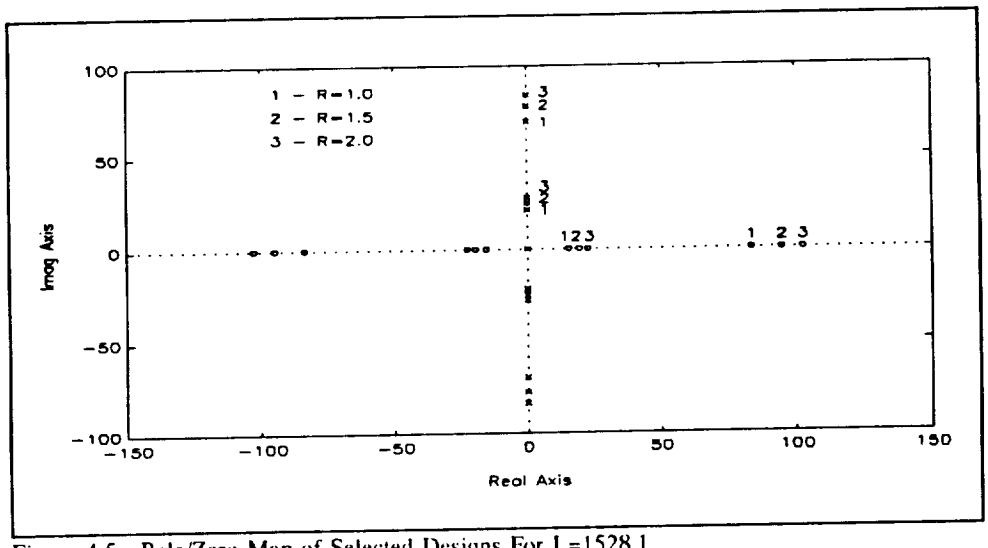

Figure 4.5: Pole/Zero Map of Selected Designs For I_y=1528.1

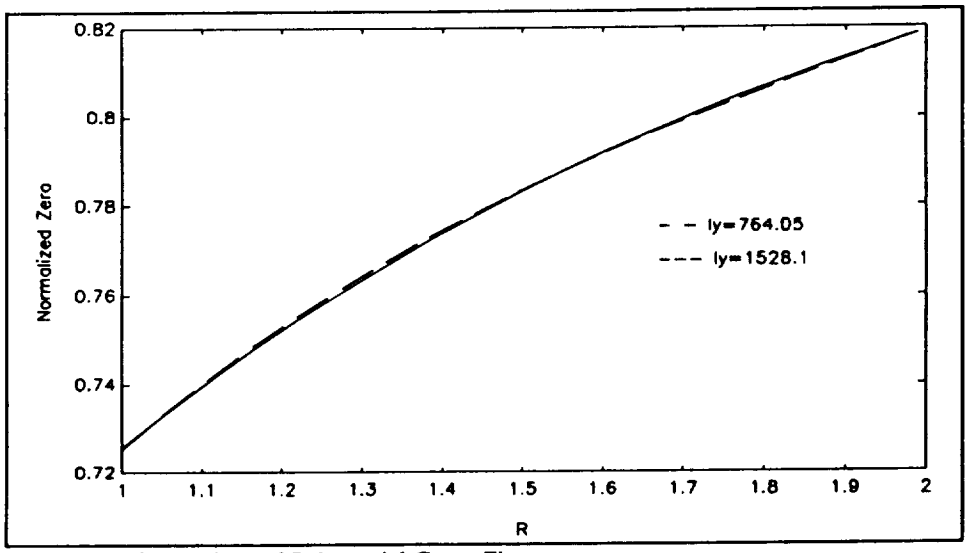

Figure 4.8: Comparison of Polynomial Curve Fits

Table 4.3: Results From Method 1

Zero Pole	NE=3 (α≤20%)	NE=5 (α≤8.6%)	NE=10 (α≤1.9%)	NE=20 (α≤0.3%)	NE=40 (α≤0.1%)	NE=80
1	13.91 13.64	13.99 15.95	13.73 16.05	13.69 15.96	13.68 15.92	13.68 15.91
2	45.57 38.08	55.99 43.24	57.28 46.19	56.91 46.21	56.84 46.14	56.83 46.11
3	121.2 88.16	122.0 85.31	134.2 92.52	133.8 93.20	133.6 93.13	133.5 93.09
4	210.8 137.5	223.2 147.5	242.9 154.9	244.7 157.0	244.2 157.0	244.1 157.0
5	357.8 219.5	383.8 234.7	382.1 233.3	389.4 237.7	388.9 237.9	388.7 237.8

Table 4.4: Results From Method 2

Zero Pole	NE=3 (α≤16%)	NE=5 (α≤4.0%)	NE=10 (α≤0.4%)	NE=20 (α≤0.1%)	NE=40 (α≤0.0%)	NE=80
1	13.09 15.57	13.49 15.82	13.64 15.89	13.67 15.90	13.68 15.91	13.68 15.91
2	53.77 38.66	56.12 45.82	56.62 46.03	56.78 46.09	56.82 46.10	56.83 46.10
3	120.4 85.88	135.1 93.17	133.0 92.90	133.4 93.03	133.5 93.06	133.5 93.06
4	233.6 154.4	234.7 148.3	243.4 156.6	243.9 156.9	244.1 156.9	244.1 156.9
5	360.6 220.3	384.6 231.1	388.2 237.4	388.3 237.7	388.6 237.7	388.6 237.8

Table 4.5: Tapered Beams With I_y=764.05

Zero Pole	A=.375 B=.375	A=.4 B=.367	A=.5 B=.333	A=.6 B=.3	A=.7 B=.267	A=.8 B=.233	A=.9 B=.2	A=1 B=.167
1	7.745 10.68	8.153 11.04	9.762 12.46	11.34 13.84	12.90 15.21	14.44 16.60	15.98 18.03	17.50 19.52
2	41.85 34.59	43.15 35.48	47.38 38.80	51.37 41.87	55.05 44.73	58.45 47.41	61.60 49.94	64.51 52.36
3	103.4 72.18	105.9 73.88	115.0 80.17	123.1 85.75	130.2 90.75	136.4 95.19	141.7 99.14	146.2 102.6
4	192.2 123.4	196.6 126.2	212.7 136.5	226.6 145.5	238.6 153.4	248.7 160.1	257.1 165.9	263.6 170.6
5	308.4 188.3	315.3 192.6	340.5 208.0	362.0 221.2	380.3 232.6	395.5 242.3	407.8 250.3	416.9 256.5

Table 4.6: Normalized Data For I_y=764.05

Zero	R=1.00	R=1.09	R=1.50	R=2.00	R=2.62	R=3.43	R=4.50	R=5.99
1	0.7252	0.7385	0.7835	0.8194	0.8481	0.8699	0.8863	0.8965
2	3.919	3.909	3.803	3.712	3.619	3.521	3.417	3.305
3	9.682	9.592	9.230	8.895	8.560	8.217	7.859	7.490
4	18.00	17.81	17.07	16.37	15.69	14.98	14.26	13.50
5	28.88	28.56	27.33	26.16	25.00	23.83	22.62	21.36

Table 4.7: Tapered Beams With I_y=1528.1

Zero Pole	A=.75 B=.75	A=.8 B=.733	A=.9 B=.7	A=1.0 B=.667	A=1.1 B=.633	A=1.2 B=.600
1	15.49 21.35	16.31 22.08	17.92 23.51	19.52 24.92	21.11 26.30	22.68 27.68
2	83.71 69.16	86.03 70.95	90.50 74.35	94.76 77.60	98.83 80.73	102.7 83.74
3	206.7 144.4	211.7 147.7	221.2 154.2	230.1 160.3	238.4 166.1	246.2 171.5
4	384.4 246.8	393.2 252.5	409.9 263.1	425.4 273.1	439.9 282.4	453.2 291.0
5	616.7 376.7	630.6 385.1	656.8 401.1	681.0 415.9	703.3 429.6	724.0 442.4

Table 4.9: ZERO Results For Uniform Beam Designs

Zero Pole	W=0.25"	W=0.5"	W=0.75"
1	5.163 7.116	10.33 14.23	15.49 21.35
NZ	0.726	0.726	0.726
2	27.90 23.06	55.80 46.12	83.71 69.19
3	68.90 48.12	137.8 96.23	206.7 144.3
4	128.1 82.28	256.2 164.6	384.4 246.8
5	205.6 125.6	411.1 251.1	616.7 376.7

Table 4.10: Variable Height Designs

Zero Pole	H=1.0"	H=1.5"	H=2.0"
1	11.34 13.84	11.34 13.84	11.34 13.84
2	51.37 41.87	51.37 41.87	51.37 41.87
3	123.1 85.75	123.1 85.75	123.1 85.75
4	226.6 145.5	226.6 145.5	226.6 145.5
5	362.0 221.2	362.0 221.2	362.0 221.2
I_y	764.05	1146.1	1528.1

The Application of Input Shaping to a System with Varying Parameters

David P. Magee, Graduate Student
Dr. Wayne J. Book, Professor
George W. Woodruff School of Mechanical Engineering
Georgia Institute of Technology
Atlanta, Georgia

Abstract

The original input shaping technique developed by Singer and Seering is summarized and a different definition for residual vibration is proposed. The new definition gives better insight into the ability of input shaping method to reduce vibration. The extension of input shaping to a system with varying parameters, e.g. natural frequency, is discussed and the effect of these variations is shown to induce vibration. A modified command shaping technique is developed to eliminate this unwanted motion.

Introduction

The industrial and environmental applications for robots with a relatively large workspace has increased significantly in the last few years. To accommodate the demands, the manipulator is usually designed with long, lightweight links which are inherently flexible. This flexibility allows the links to store potential energy which is returned to the system in the form of kinetic energy. Therefore, the end-point vibration, which affects the uncertainty in end-point position, is directly related to the flexibility of the links.

Many different methods, both passive and active, have been investigated to eliminate unwanted oscillation to improve end-point positioning capabilities. The most crude passive approach to eliminate vibration is to simply wait for vibrations to stop after a desired motion. NASA originally used this method on their Space Shuttle Remote Manipulator System but found it to be very costly in task completion time requirements. Other passive approaches include applying a thin layer of visco-elastic material to absorb energy, using piezo-resistive films to resist beam motion and various vibration absorption techniques [1,2,3].

The majority of the present day techniques involve active control structures to minimize end-point vibration. Different states of the system are measured and conventional feedback schemes are used to control the vibration. Hastings and Book [4] extended active control methods by including strain feedback in the control structure. They showed that strain feedback can reduce residual vibration during settling time. However, they conclude that the vibrations are inevitable with a feedback control scheme because feedback control signals contain high frequency components, which excite the system resonances.

Another method to reduce vibration is the use of inertial devices. Montgomery, Ghosh and Kenny [5] propose torque-wheel actuators to reduce overshoot in the Space Shuttle Remote

Manipulator. Their results indicate that the wheel can produce a vibration of significant amplitude to diminish the original unwanted vibration. Lee and Book [6] are studying the effects of inertial forces to suppress vibration by mounting a small robot at the tip of a large, flexible robot. Using deflection rate control, the small robot generates damping forces to accommodate the inertial forces generated at the tip.

The technique that is discussed in this paper involves the modification of a command signal so that the system resonances are not excited. The idea of command altering is not a new one. O.J.M. Smith [7] suggested the use of posicast control which takes a step of a given amplitude and separates it into two smaller steps, one of which is separated in time. This method was shown to reduce the settling time of the system. Meckl and Seering [8] examined the construction of the input from a series expansion of ramped sinusoid functions with coefficients chosen to minimize a spectral magnitude. The results were reduction in residual vibration even for variations in resonant frequencies.

Singer and Seering [9,10,11] presented a method of generating shaped command inputs that utilizes system characteristics. Each sample of the desired input is transformed into a new set of impulses that do not excite the system resonances. This procedure, in effect, filters out frequency components near the system's resonance to avoid vibration during motion. However, their experiments were limited to systems with constant parameters. The ability of the method to accommodate slight deviations in system parameters is handled by the derivation of robustness constraints. To fully appreciate the method, a more detailed discussion is warranted.

The Input Shaping Technique

The original input shaping method developed by Singer and Seering is best explained by considering the motion of a flexible system as the linear combination of flexible and rigid body motion. The rigid body motion can be modeling using conventional methods, e.g. Newton, Lagrange, etc., and consider representing the flexible motion as a simple, second-order system. The vibratory response of a linear, time-invariant, underdamped second-order system to an impulse can be written as

$$x(t) = \frac{A\,\omega_n e^{-\zeta\omega_n(t-t_0)}}{\sqrt{1-\zeta^2}} \sin\left(\omega_n\sqrt{1-\zeta^2}\,(t-t_0)\right) \qquad (1)$$

where A is the amplitude of the impulse, ω_n is the natural frequency of the system, ζ is the damping ratio of the system, t is the time and t_0 is the time when the impulse occurs. Since the input shaping technique generates a set of new impulses, the response of the second-order system to two impulses can be expressed as

$$x(t) = B_1\sin(\alpha t + \phi_1) + B_2\sin(\alpha t + \phi_2) \qquad (2)$$

where

$$B_k = \frac{A_k \omega_n}{\sqrt{1-\zeta^2}} e^{-\zeta \omega_n (t - t_{0k})} \tag{3}$$

$$\alpha = \omega_n \sqrt{1-\zeta^2} \tag{4}$$

$$\phi_k = -\omega_n t_{0k} \sqrt{1-\zeta^2}. \tag{5}$$

The response of the system to the two impulse input can be simplified to yield

$$x(t) = B_{amp} \sin(\alpha t + \psi) \tag{6}$$

$$B_{amp} = \sqrt{[B_1 \cos(\phi_1) + B_2 \cos(\phi_2)]^2 + [B_1 \sin(\phi_1) + B_2 \sin(\phi_2)]^2} \tag{7}$$

$$\psi = \tan^{-1}\left(\frac{B_1 \sin(\phi_1) + B_2 \sin(\phi_2)}{B_1 \cos(\phi_1) + B_2 \cos(\phi_2)}\right). \tag{8}$$

Since the system is linear and time-invariant, the results from Equations (7) and (8) can be generalized to the N impulse case. The resulting amplitude and phase for the response are

$$B_{amp} = \sqrt{\left[\sum_{k=1}^{N} B_k \cos(\phi_k)\right]^2 + \left[\sum_{k=1}^{N} B_k \sin(\phi_k)\right]^2} \tag{9}$$

$$\psi = \tan^{-1}\left(\frac{\sum_{k=1}^{N} B_k \sin(\phi_k)}{\sum_{k=1}^{N} B_k \cos(\phi_k)}\right). \tag{10}$$

Since the purpose of the input shaping method is to eliminate vibration, the amplitude of vibration given in Equation (9) must equal zero after the last input impulse occurs in time. This only happens if both the squared terms are independently zero since the sine and cosine functions are linearly independent. The resulting equations are

$$B_1 \cos(\phi_1) + B_2 \cos(\phi_2) + \ldots + B_N \cos(\phi_N) = 0 \tag{11}$$

$$B_1 \sin(\phi_1) + B_2 \sin(\phi_2) + \ldots + B_N \sin(\phi_N) = 0. \tag{12}$$

Simplifying Equations (11) and (12) yields the zeroth-order constraint equations given by

$$\sum_{k=1}^{N} A_k e^{-\zeta \omega_n (t_N - t_{0k})} \cos(\omega_n \sqrt{1-\zeta^2}\, t_{0k}) = 0 \tag{13}$$

$$\sum_{k=1}^{N} A_k e^{-\zeta \omega_n (t_N - t_{0k})} \sin(\omega_n \sqrt{1-\zeta^2}\, t_{0k}) = 0. \tag{14}$$

For the constraint equations to produce the correct impulse sequence to eliminate vibration, the natural frequency and damping ratio of the system must be exact. Since these system characteristics are never precisely known, a robustness constraint is added. The robustness constraints are found by taking the partial derivatives of Equations (13) and (14) with respect to ω_n or ζ and setting the result equal to zero. Higher derivative constraints are obtained by differentiating the equations to the desired order. The mth-derivative robustness constraints are

$$\sum_{k=1}^{N} A_k (t_{0k})^m e^{-\zeta \omega_n (t_N - t_{0k})} \cos(\omega_n \sqrt{1-\zeta^2}\, t_{0k}) = 0 \tag{15}$$

$$\sum_{k=1}^{N} A_k (t_{0k})^m e^{-\zeta \omega_n (t_N - t_{0k})} \sin(\omega_n \sqrt{1-\zeta^2}\, t_{0k}) = 0. \tag{16}$$

The length of the impulse sequence is now determined by the number of unknowns in a given set of constraint equations. For any given set, there will always be two more unknowns than equations. To alleviate this dilemma, the starting time of the first impulse is chosen to be time zero and the amplitudes of the impulses are normalized so that they sum to unity. This particular normalization ensures that the overall amplitude of the new impulse sequence is the same as the amplitude of the desired input command.

Example of Two Impulse Case

For the two impulse case, the zeroth-order constraint equations are utilized, which are

$$B_1 \cos(\phi_1) + B_2 \cos(\phi_2) = 0 \tag{17}$$

$$B_1 \sin(\phi_1) + B_2 \sin(\phi_2) = 0. \tag{18}$$

Since any equation involving sines and cosines is transcendental, there are an infinite number of possible solutions to Equations (17) and (18). Therefore, only the solution that yields the shortest time duration and a positive amplitude for all the impulses is chosen. The solution is

$$A_1 = \frac{1}{1+M} \tag{19}$$

$$t_{01} = 0 \tag{20}$$

$$A_2 = \frac{M}{1+M} \tag{21}$$

$$t_{02} = \frac{\pi}{\omega_n \sqrt{1-\zeta^2}} \tag{22}$$

where

$$M = e^{-\frac{\zeta \pi}{\sqrt{1-\zeta^2}}}. \tag{23}$$

Equation (22) states that the second impulse occurs in time at one-half the damped period of the system. This seems reasonable to apply an impulse to oppose the vibration of the system. The ability of the input shaping method to eliminate vibration can be demonstrated graphically. Consider the input given in Figure 1 whose characteristics are given in Equations (19) thru (22).

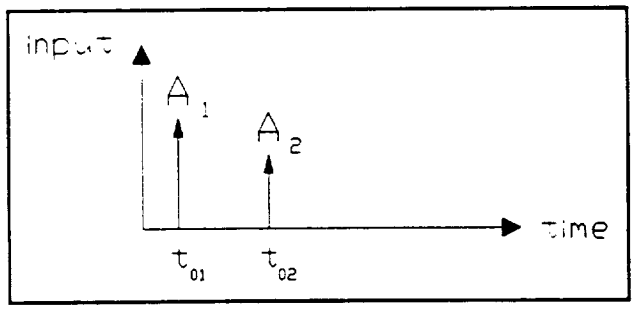

Figure 1. Two Impulse Input

The second-order system response to each of the impulses in Figure 1 is shown in Figure 2.

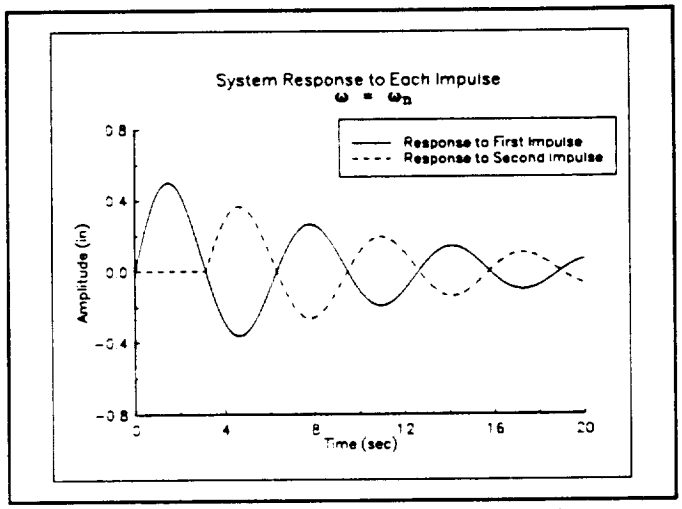

Figure 2. System Response to Each Impulse

Since the system is linear and time-invariant, a linear combination of two inputs results in a response that is a linear combination of the two responses. Therefore, the net system response to the two impulse input is shown in Figure 3. Since the natural frequency and damping ratio

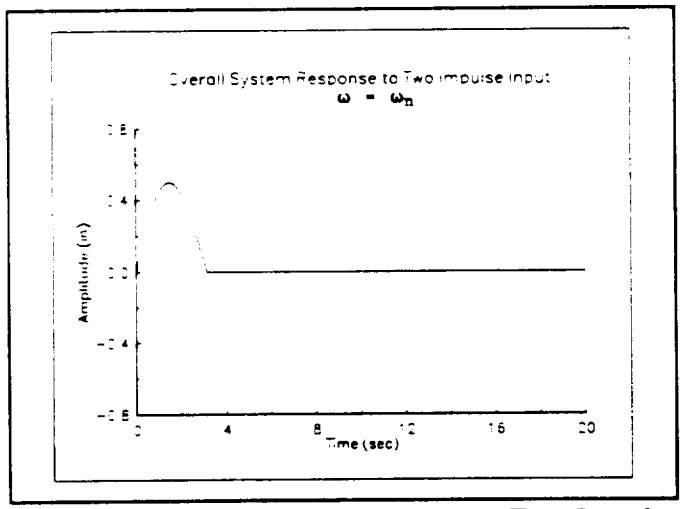

Figure 3. Overall System Response to Two Impulse Input

are exact, there is no vibration of the system after the second impulse occurs. The flexible motion has been eliminated and all that remains is rigid body motion.

Robustness of Constraint Equations

The previous example demonstrated the ability of the input shaping method to eliminate vibration when the natural frequency and damping ratio of the system were known exactly. For most physical systems, the exact parameters are seldom known. Thus, there is some residual vibration after the last impulse has occurred. To determine the amount of residual vibration, a new vibration error expression must be defined. The error, denoted *err*, is expressed as the ratio of the actual multiple impulse response magnitude to the actual impulse response magnitude of the second-order system. The error expression is defined only for time after the multiple impulse input has occurred to ensure that the system has received identical amplitude inputs, i.e. the inputs sum to the same value. Mathematically, the vibration error is written as

$$err = \frac{|x_{ka}(t)|}{|x_a(t)|} \quad , \quad for \quad t \geq t_{0k} \tag{24}$$

where k is the number of impulses. The residual vibration is just the vibration error expressed as a percentage.

The deviation of the actual system parameters from the design parameters can now be quantified using Equation (24). By studying the deviations in natural frequency and damping ratio from the design parameters, their effects on vibration error can be better understood. To demonstrate this point, again considered the two impulse input case. The vibration error from Equation (24) is found to be

$$\frac{|x_{2a}(t)|}{|x_a(t)|} = \left| \frac{1}{M+1} \sqrt{1 + 2M^{\left(1-\frac{\omega_a}{\omega_n}\right)} \cos\left(\frac{\omega_a}{\omega_n}\pi\right) + M^{2\left(1-\frac{\omega_a}{\omega_n}\right)}} \right| \tag{25}$$

where ω_a is the actual natural frequency of the system and ω_n is the design natural frequency of the system. Figure 4 shows the vibration error as a function of normalized frequency, ω_a/ω_n and Figure 5 displays Singer's original vibration error. The two principal differences between the definitions are evident when comparing the figures:

1. The magnitudes achieved by the residual vibration

2. The behavior of the residual vibration with respect to damping ratio

From Singer's definition, the magnitude of the residual vibration never exceeds 100%. This phenomenon implies that the input shaping method will never increase the residual vibration of the system no matter the variation in natural frequency. Clearly, this is cannot be the case. One can envision applying the second impulse at a time equal to the damped period of the system. Figure 6 reveals a second-order system response to a single impulse input compared with a two impulse input when the actual natural frequency is twice the design natural frequency. The residual vibration after the second impulse is actually worse than if the system had only been given the single impulse. Therefore, the input shaping method can have a detrimental effect

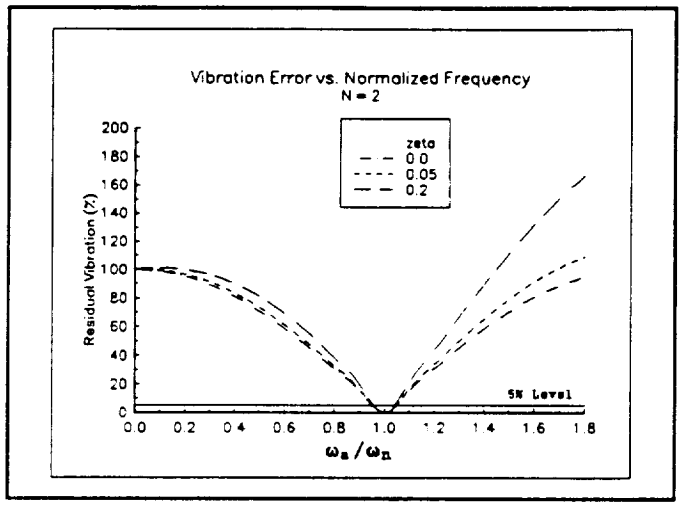

Figure 4. Vibration Error vs. Normalized Frequency - Two Impulse Input

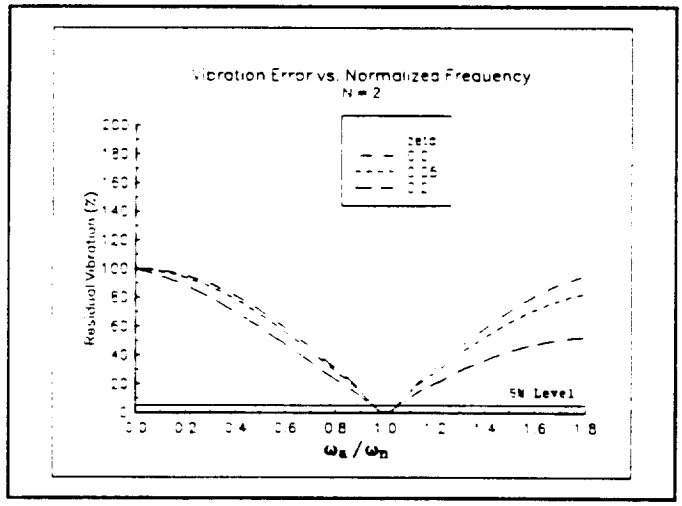

Figure 5. Vibration Error vs. Normalized Frequency - Singer's Definition

when large errors in natural frequency occur.

The second difference deals with the relationship between the damping ratio and the residual vibration. The new definition shows that the residual vibration increases for an increase in damping ratio. This fact may seem incorrect since the overshoot of a second-order system decreases with an increase in damping ratio. However, manipulation of Equation (1) for different values of damping ratio (at a constant value of natural frequency) reveals that the amplitude of the impulse response increases for larger values of damping ratio.

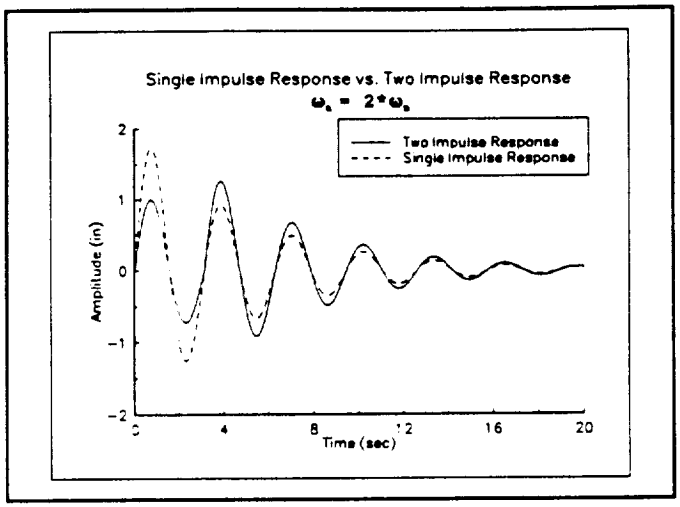

Figure 6. Single Impulse Response vs. Two Impulse Response

One final note regarding the vibration error is the robustness of the two impulse input. Singer defines an acceptable vibration error level of less than 5% residual vibration for the second-order system. After reviewing Figure 4, the two impulse input is robust only for a frequency variation of less than 5%. To improve the robustness with respect to natural frequency, more impulses must be used. By solving the higher order derivative constraints mentioned previously, the amplitudes and starting times of more impulses can be found. After solving set of equations, the vibration error can be calculated. The vibration error graphs for the case of three and four impulses are shown in Figures 7 and 8, respectively. Notice that the robustness for variations in natural frequency increases for more impulses but there is a larger penalty in residual vibration if the parameters are outside the acceptable level.

The robustness with respect to damping ratio can also be pursued by evaluating the vibration error equation for variations in damping ratio. Singer states that the higher order derivative constraints also satisfy variations in damping ratio so the derivation will not be addressed here. The only point to make is that large variations in damping ratio do not have a significant effect on the residual vibration. This fact is comforting since the damping ratio of a complex system can be difficult to measure.

Position Dependent Parameters

The robustness of the constraint equations demonstrated the ability of the input shaping method to reduce vibrations even with deviations from the design parameters. However, the method does not consider the issue of changing system parameters. For many flexible, robot systems, the natural frequency and damping ratio are functions of position, e.g. joint angles. Therefore, a modified command shaping technique is developed to accommodate this deficiency.

To develop this new method, the implementation of the input shaping technique to a discrete-time system is presented. Figure 9 shows a simple block diagram of the input shaping

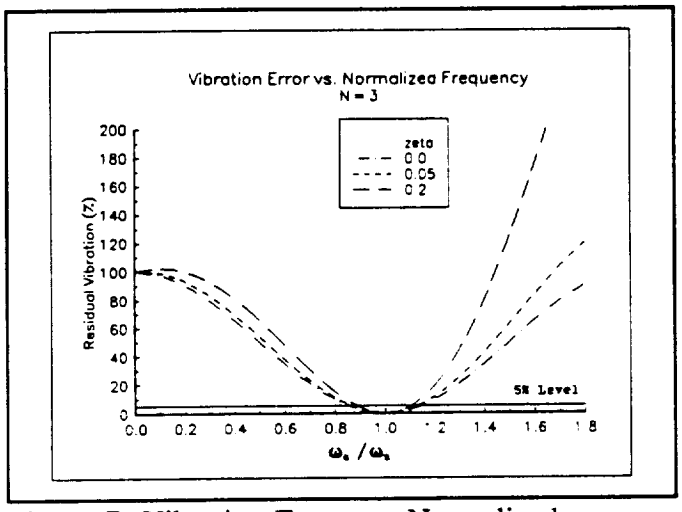

Figure 7. Vibration Error vs. Normalized Frequency - Three Impulse Input

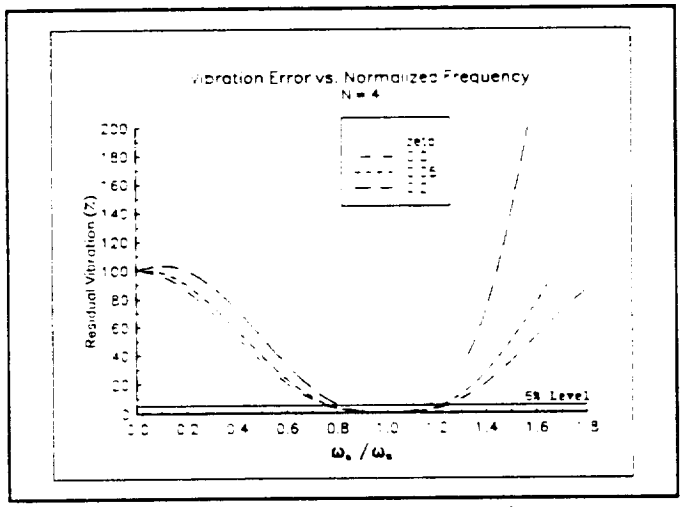

Figure 8. Vibration Error vs. Normalized Frequency - Four Impulse Input

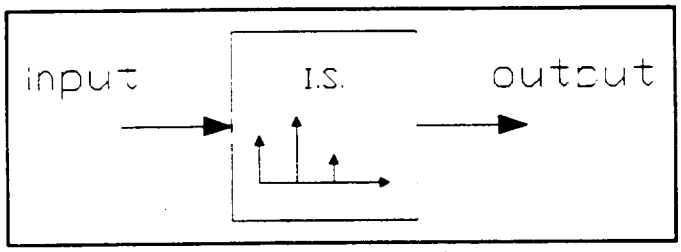

Figure 9. Input Shaping Block Diagram

method. For each sample of the desired input, N output impulses are generated. The output impulses are equally spaced in time with a continuous-time period, denoted *delT*,

$$delT = \frac{\pi}{\omega_n \sqrt{1 - \zeta^2}} \tag{26}$$

which is a function of both the natural frequency, ω_n, and damping ratio, ζ. To utilize this time period information in a discrete-time system, the continuous-time data must be represented in discrete-time. From discrete-time signal processing, a continuous-time signal, $x(t)$, is represented mathematically as a sequence of numbers, $x[n]$, where n is strictly an integer. To transform the continuous-time period *delT* into a discrete time period *deln*, the sampling rate of the discrete-time system, f_s, is used. The equation to perform this transformation is

$$deln = int(delT * f_s) \tag{27}$$

where the *int* function truncates its argument to an integer.

For the input shaping method, the discrete-time period, *deln*, never changes because the system parameters are assumed constant. But when the input shaping method is applied to a system that has time varying parameters, the continuous-time period, *delT*, becomes time varying as well. A significant change in *delT* will result in a change in the discrete-time period, *deln*, which produces an undesirable vibration in the system. The amount of change in the continuous period that causes this change in the discrete period is a function of sampling rate since *deln* is strictly an integer.

For example, consider the input shaping method shown in Figure 9 that produces four new impulses for each sample of the desired input. Assuming that the discrete-time period evaluates to an integer value of four, the method would produce a steady-state impulse output shown in Figure 10. Each output impulse is designated $\{a,b\}$ where a indicates the discrete-time location of the input sample responsible for the four output impulses and b indexes the four resulting output impulses. Now assume that the system configuration has changed enough to alter the value of the discrete-time period. Figure 11 shows the steady-state impulse output for a change in the discrete-time period, *deln*, from four to five. After examining Figure 11, it is obvious that the change in *deln* has caused gaps in the output for discrete values of n. At $n=4$, for example, only three impulses are contributing to the overall output. To make matters worse, this problem is repeated five more times at a discrete-time period near the system's natural period. This phenomenon induces a vibration into the system that is caused solely by the application of the input shaping method to a system with time varying parameters.

This induced vibration is also present when the value of *deln* decreases. Consider a change in *deln* from five to four. The resulting steady-state impulse output is shown in Figure 12. For this situation, a surplus of output impulses is generated at a discrete-time period near the system's natural period. These extra impulses also cause a vibration that is produced by the input shaping method.

To eliminate the induced vibration, a modified command shaping method is proposed to make the impulse output more uniform when a change in *deln* is encountered. To compensate for a change in the discrete-time period, extra impulses are added for an increase in *deln* and impulses are removed for a decrease in *deln*. The choice of which impulses are affected is based

on the number of output impulses from the shaping algorithm and the old and new values of the discrete-time period.

Modified Command Shaping

The modified command shaping method can be explained by designating the discrete-time value when the discrete period increases as $n=0$. For the next N-1 samples of the input, i.e. $0 \leq n \leq N$-2, the modified command shaping technique shapes each sample using both the old and new values of *deln* to create a smooth steady-state impulse output. Using the new value of *deln*, the input sample is shaped to create N output impulses that are added to the overall output at their respective discrete-time values. Using the old value of *deln*, the same input sample is also shaped to create N output impulses. However, only the last N-(n+1) output impulses are added to the steady-state output at their respective discrete-time values. For discrete-time values of $n \geq N$-1, each sample of the input is shaped normally using the new value of *deln* to generate the N output impulses.

The modified command shaping method also works for a decrease in the discrete-time period, *deln*. For this situation, the input sample is shaped only once using the new value of *deln* to produce the four output impulses. Instead of adding all four of the output impulses, only the first (n+1) output impulses are added to the steady-state output at their respective discrete-time values. By manipulating the overall output in this way, the extra impulses that are added for the case when *deln* increases are the same impulses that are removed when *deln* decreases.

One final case to consider is when the value of *deln* changes more than once within one discrete-time period. For this situation, a new modified technique must be devised. For instance, if the discrete-time period length changes from one value to another and back again, the best method to smooth the steady-state output may be to ignore the change in discrete period if it is relatively short.

To understand the modified command shaping procedure, consider the example given in Figure 11. The value of *deln* increases from four to five for this input shaping scheme that produces four output impulses. Since N=4 for this case, the next three (i.e. N-1) input samples will be shaped twice. At discrete-time n=0, the input sample is shaped using the new value of *deln* (i.e. 5) to create four (i.e. N) output impulses that are added to the overall output. At the same discrete-time value, the input sample is shaped using the old value of *deln* (i.e. 4) to create four (i.e. N) output impulses. However, only the last three (i.e. N-(n+1)) impulses are added to the overall output at their respective discrete-time values. For the next discrete-time value, i.e. n=1, the input sample is shaped using the new value of *deln* to create the usual four output impulses that are added to the overall output. When the input sample is shaped using the old value of *deln*, only the last two (i.e. N-(n+1)) output impulses are added to the general output. This process of shaping the input samples twice is repeated until the discrete-time value, n, is greater that N-2. After $n > N$-2, the shaping continues normally using only the new value of *deln* to produce the output impulses. The steady-state impulse output for an increase in discrete-time period using the modified command shaping is shown in Figure 13. The impulses due to the modified method are darkened to show emphasis only.

The application of the modified command shaping method to a decrease in discrete-time period is much simpler. Considering the example in Figure 12, the steady-state impulse output from the modified method is given in Figure 14. The impulses that are created but not added

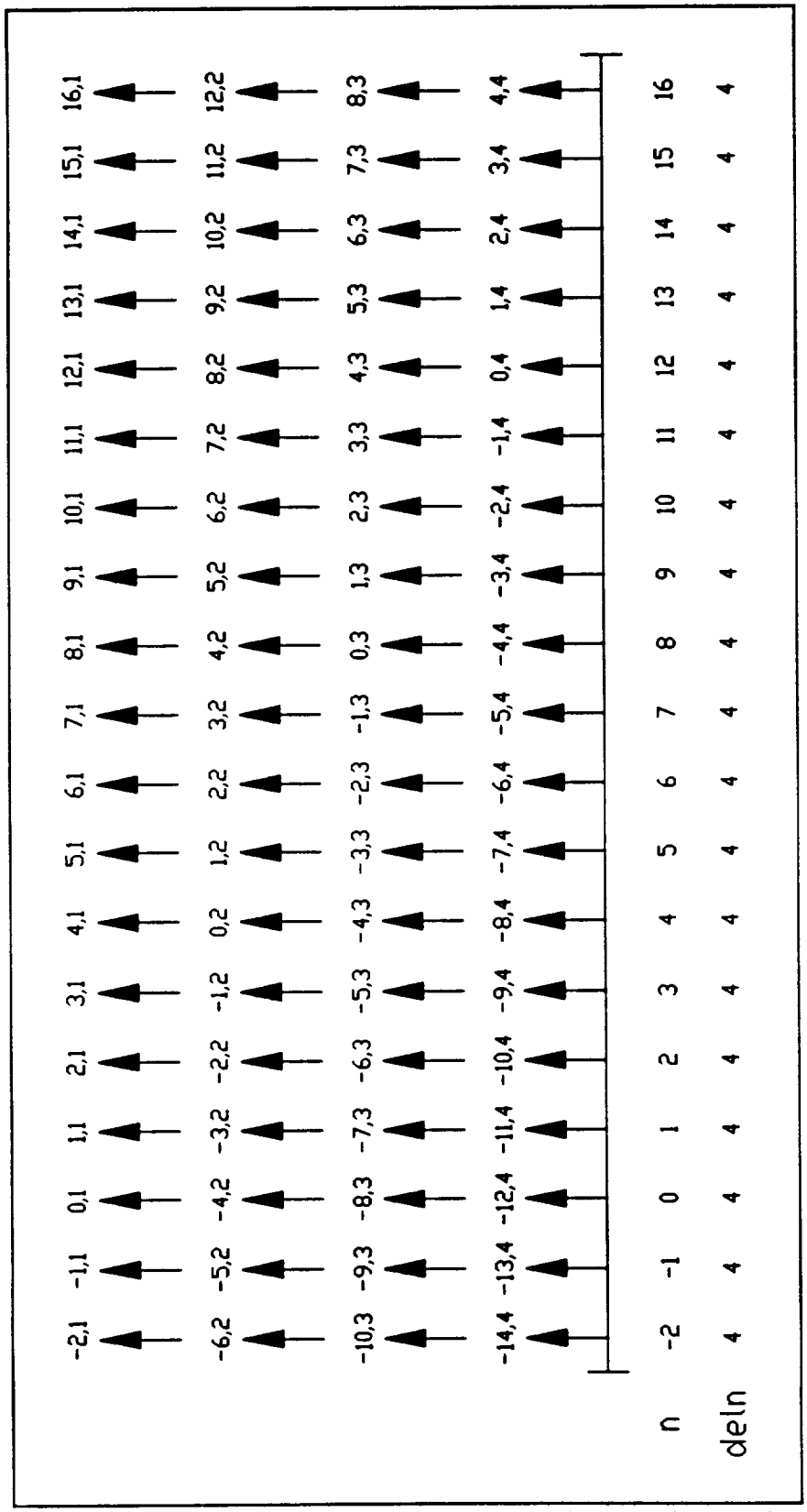

Figure 10. Steady-State Output for Constant Discrete-Time Period Using Input Shaping

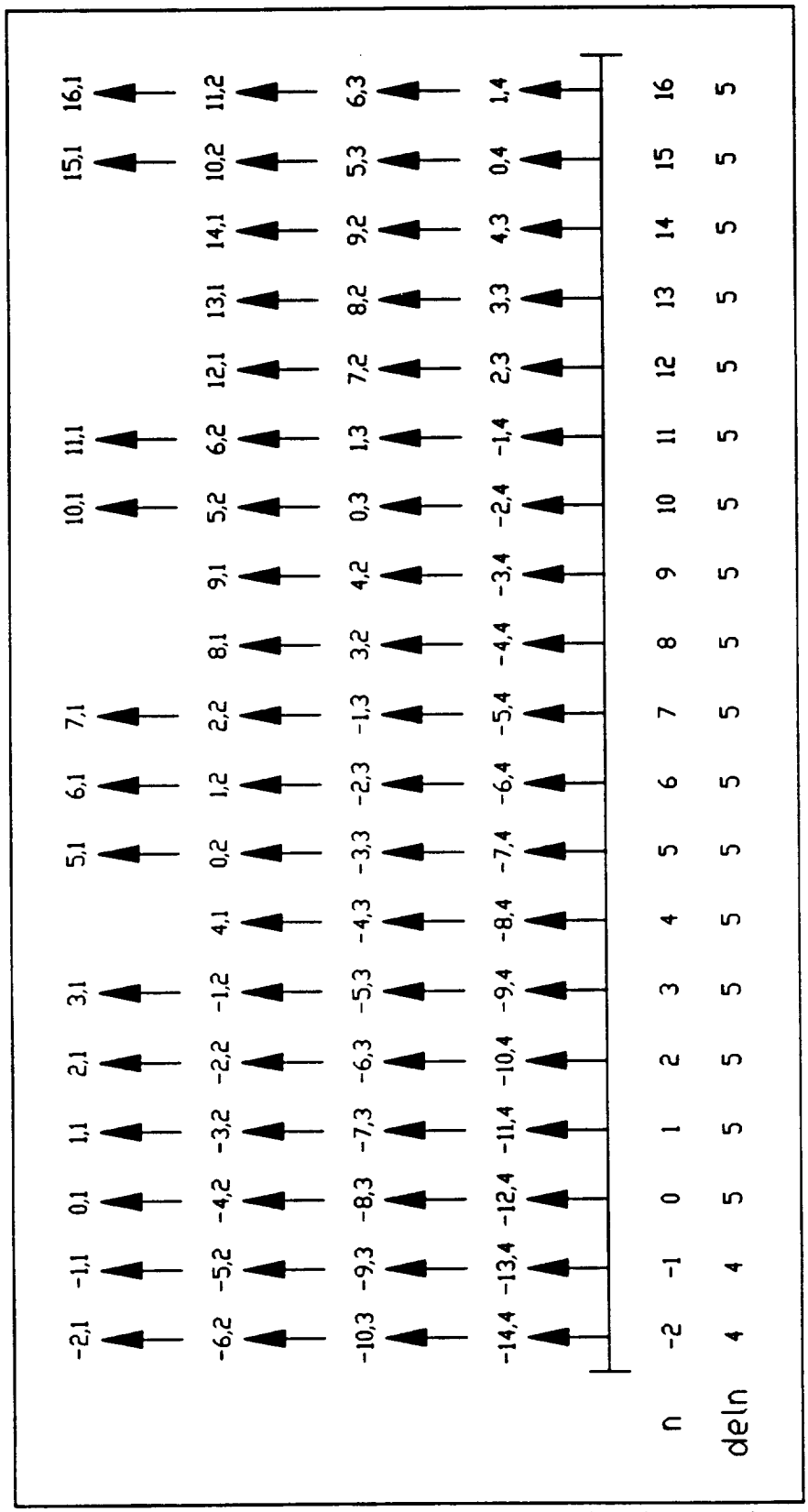

Figure 11. Steady-State Output for an Increase in Discrete-Time Period Using Input Shaping

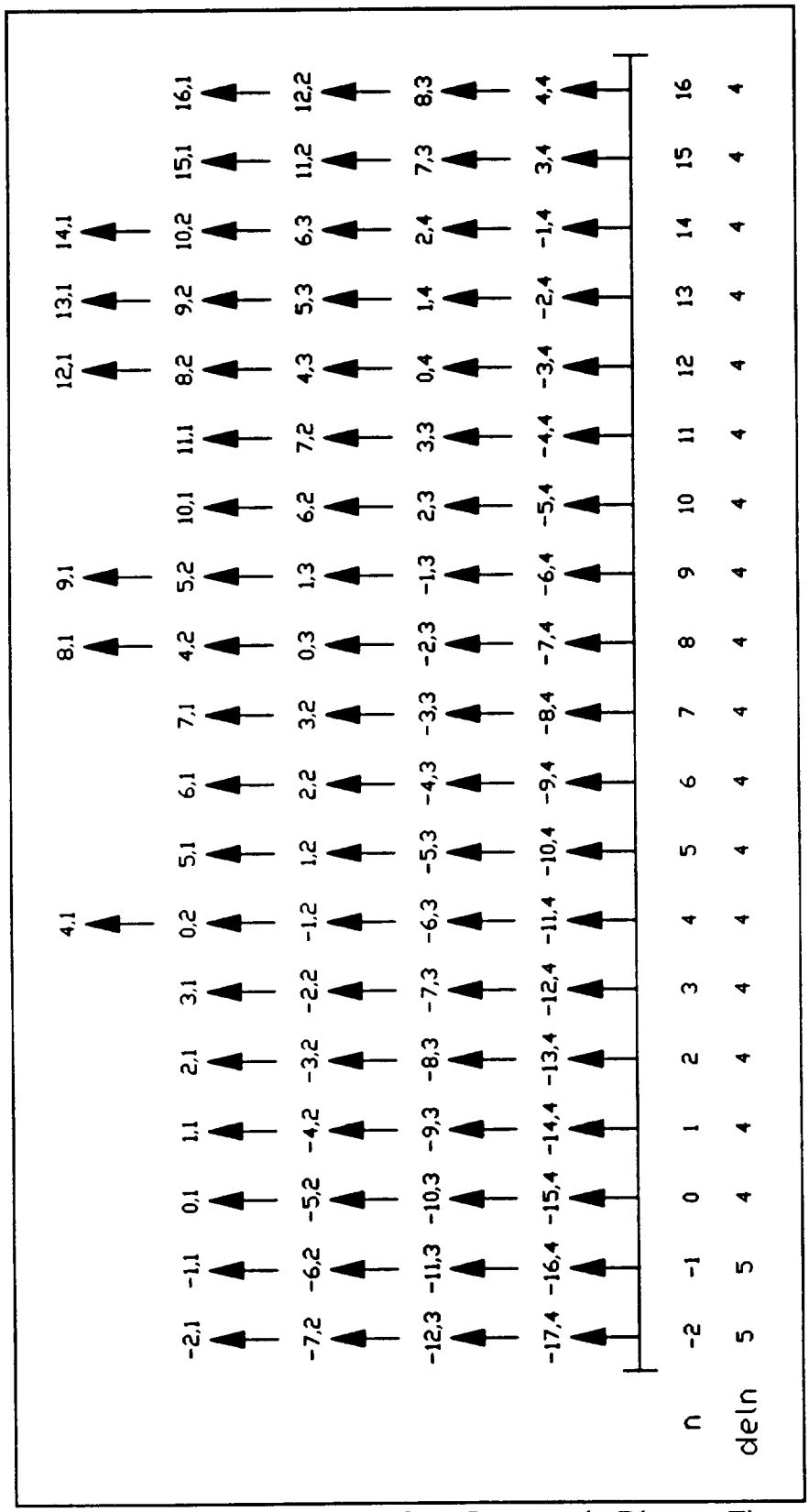

Figure 12. Steady-State Output for a Decrease in Discrete-Time Period Using Input Shaping

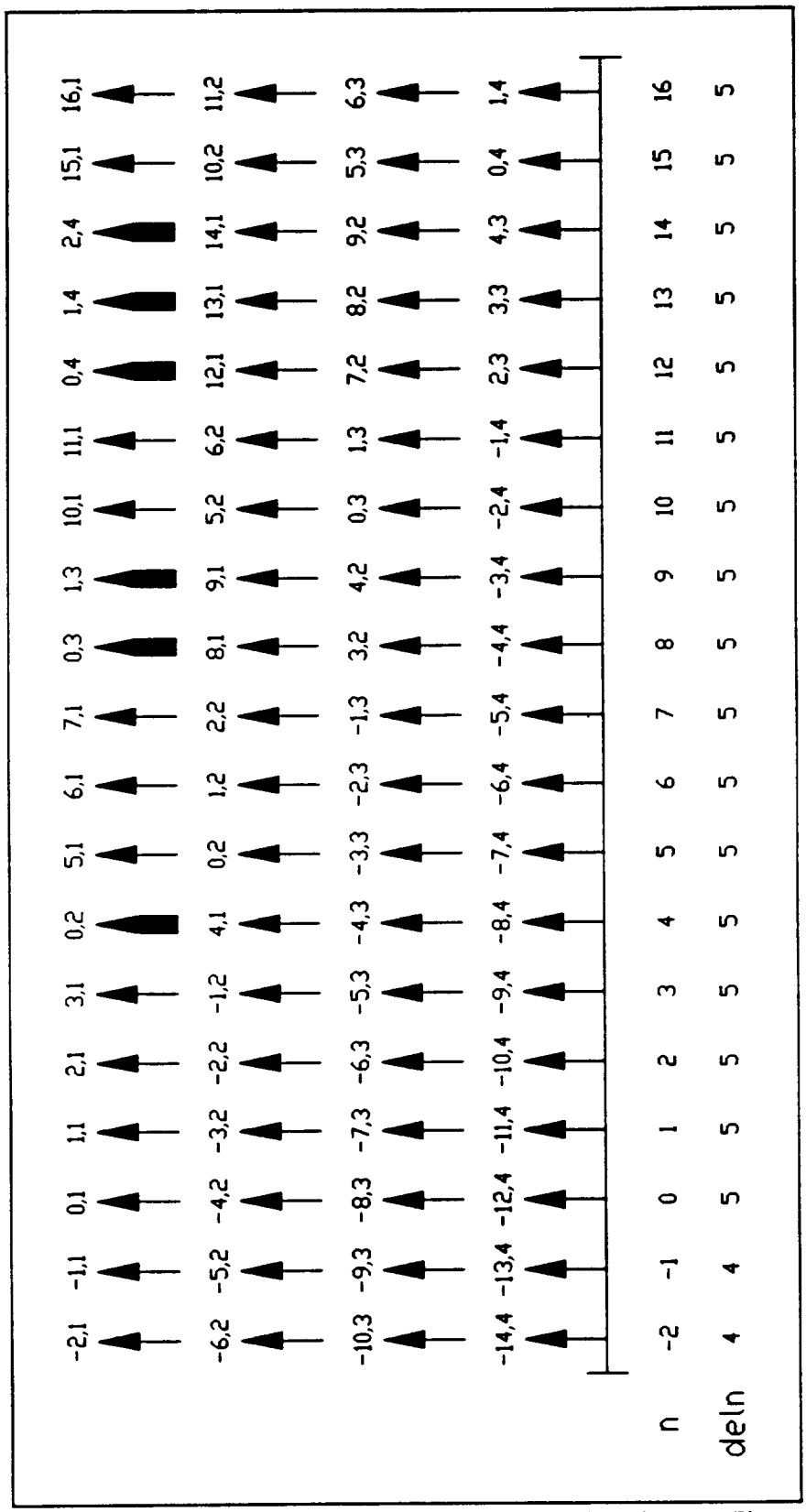

Figure 13. Steady-State Output for an Increase in Discrete-Time Period Using Modified Command Shaping

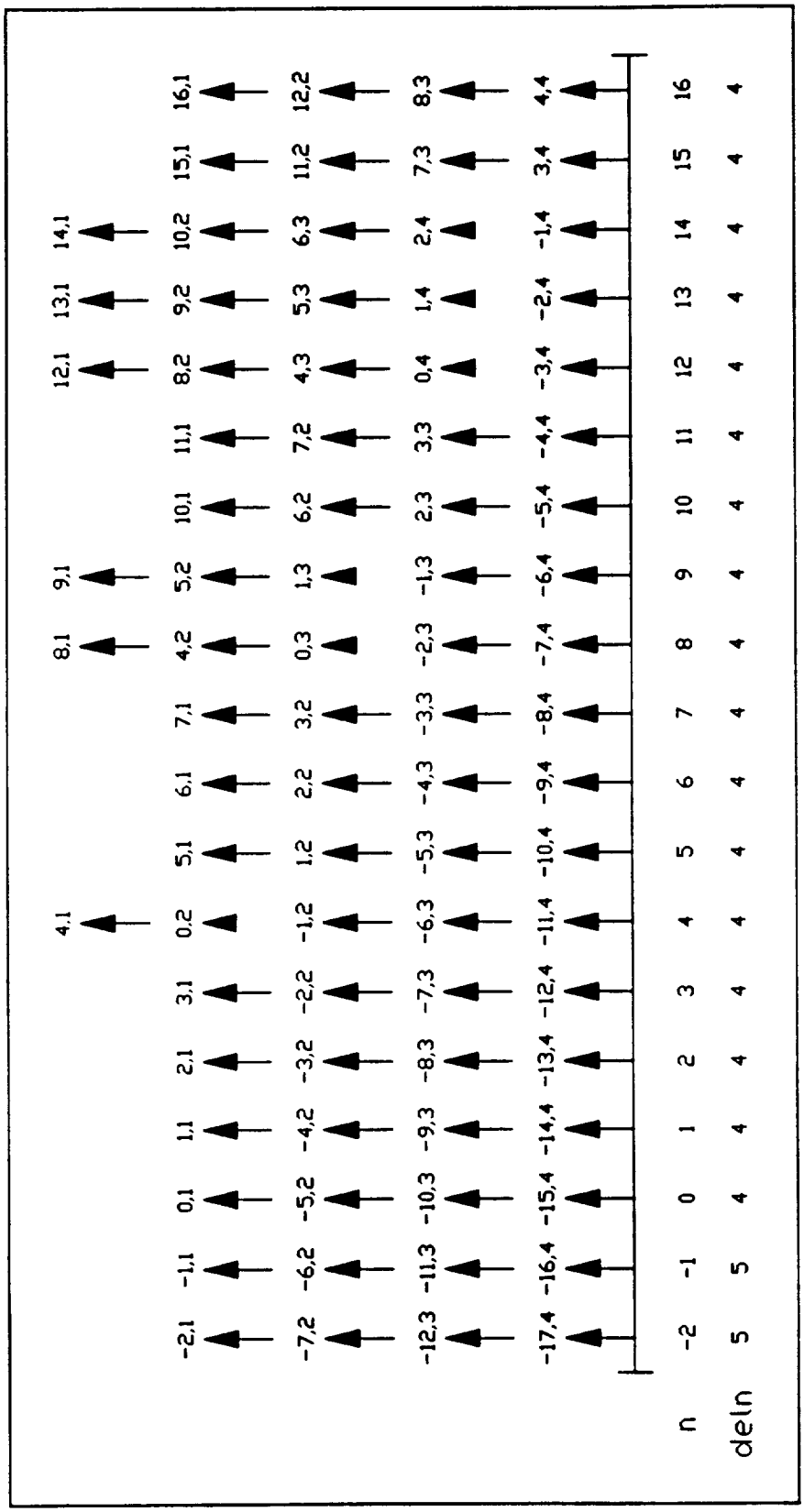

Figure 14. Steady-State Output for a Decrease in Discrete-Time Period Using Modified Command Shaping

are drawn in the figure without tails to distinguish them from the normal impulses. Notice that the extra impulses that are added for the increase in discrete-time period are the same impulses, i.e. the same indices, that are eliminated for a decrease in discrete-time period. Although the amplitudes of the impulses are not exactly the same (since they originated from different samples of the desired input), this method provides a unique means for maintaining continuity of the steady-state output impulses.

Experimental Verification of Induced Vibration

To verify that the input shaping method does induce vibration for variations in discrete-time period, the method was applied to an existing adaptive P.D. control strategy developed by Yuan [12] that controls a two DOF flexible manipulator (RALF) located at Georgia Tech. The block diagram of the comprehensive control scheme is shown in Figure 15.

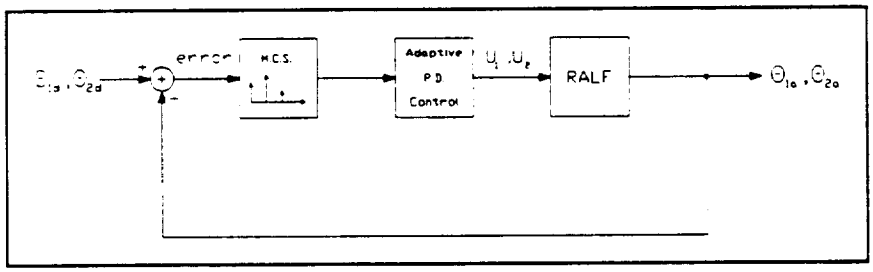

Figure 15. Block Diagram of Control System

The main control unit is a MicroVAX II containing A/D boards that can sample a single channel at 6000 Hz. However, the boards are limited to 300 Hz if multiple channels are accessed. After the computation time of the control routines is considered, the sampling frequency is reduced to 50 Hz. This sampling rate is acceptable since the first natural frequency of RALF that is to be controlled ranges from 3.7 to 5.5 Hz.

To demonstrate the elimination of the induced vibration, a desired trajectory in joint space is precomputed to ensure an equivalent basis for comparison. For this example, the desired path is a circle in cartesian space that is three feet in diameter with a period of nine seconds. An accelerometer is mounted at the tip of the robot to measure transverse vibration of the second link. The robot is commanded to follow the desired trajectory eight times which allows for reliable averaging of the data. A HP Signal Analyzer records the time response of the accelerometer and computes the frequency response of the data.

Figure 16 shows a comparison of the frequency response between the original P.D. control routine without command shaping and the original input shaping method of Singer's substituted for the modified command shaping method in Figure 15. Notice that the frequency response of the input shaping method is greater than for the P.D. routine alone. At the frequency range the input shaping method is designed to control (3.7-5.5 Hz), the response is 12 dB larger. This is due to a change in the discrete-time period which induces vibration at the system resonances. It is also worth pointing out that the second resonance of RALF occurs near 10 Hz and is evident in the frequency response.

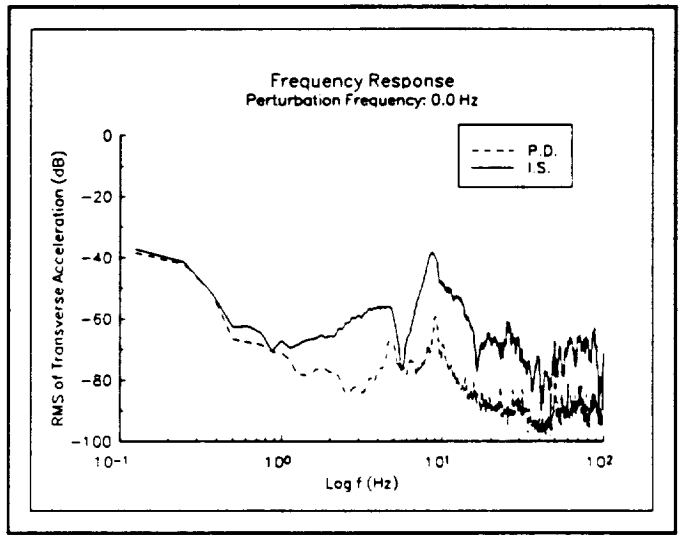

Figure 16. Frequency Response of RALF
P.D. vs. Input Shaping

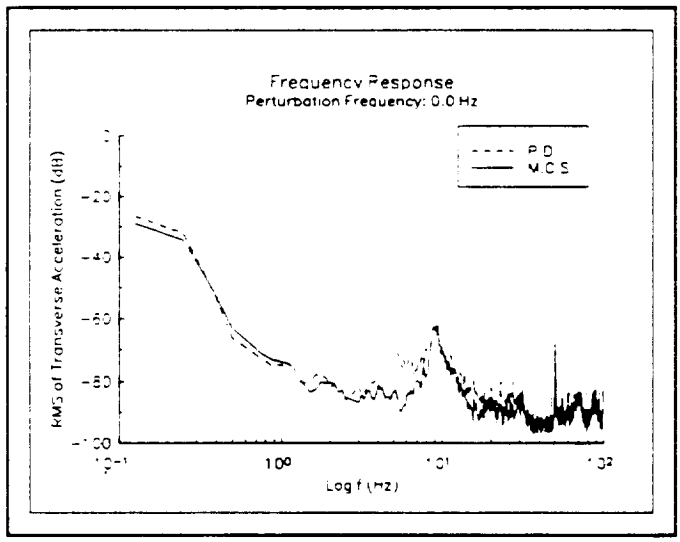

Figure 17. Frequency Response of RALF
P.D. vs. Modified Command Shaping

Figure 17 compares the frequency response between the P.D. routine and the modified command shaping method. The modified command shaping has reduced the magnitude of the resonant vibration by 20 dB compared to the original P.D. routine. Therefore, this modified method reduced the vibration by nearly 32 dB over the input shaping method. Again, this increase in performance is due to the inability of the input shaping method to accommodate a change in the discrete-time period. A visualization method that clearly shows the induced vibration can be found in [13].

Conclusion

The original input shaping method developed by Singer and Seering was presented and robustness criterion described. A different vibration error expression was presented and shown to better represent the ability of the method to reduce residual vibration. The input shaping method was shown to induce vibration in systems with varying parameters and a modified command shaping technique was developed. The ability of the modified method to eliminate the induced vibration was shown using frequency response analysis of the transverse vibration of the tip of a flexible manipulator.

References

1. Alberts, T.E., Hastings, G.G., Book, W.J. and Dickerson, S.L., "Experiments in Optimal Control of a Flexible Arm with Passive Damping," *Fifth VPI&SU/AIAA Symposium on Dynamics and Control of Large Structures*, Blacksburg, VA, 1985.

2. Bailey, T. and Hubbard, J.E.,"Distributed Piezoelectric-Polymer Active Vibration Control of a Cantilever Beam," *Journal of Guidance and Control*, September-October, 1985, pp. 605-611.

3. Tewani, S.G., Walcott. B.L. and Rouch, K.E., "Active Optimal Vibration Control using Dynamic Absorber," *Proceedings of the 1991 International Conference on Robotics and Automation*, Sacramento, CA, pp.1182-1187.

4. Hastings, G.G. and Book, W.J., "Experiments in the Optimal Control of a Flexible Manipulator," *Proceedings of the 1988 American Control Conference*, Boston, MA, pp.728-729.

5. Montgomery, R.C., Ghosh, D. and Kenny, S., "Analytic and Simulation Studies on the Use of Torque-Wheel Actuators for the Control of Flexible Robotic Arms," to appear in the 1991 ASME Winter Annual Meeting, Atlanta, GA.

6. Lee, S.H. and Book, W.J., "Use of End-Effector Inertial Forces for Damping the Vibration of a Large Arm," *Proceedings of the 1989 American Control Conference*, Philadelphia, PA, pp.1377-1380.

7. Smith, O.J.M., "Feedback Control Systems," McGraw-Hill, 1958.

8. Meckl, P.H. and Seering, W.P., "Reducing Residual Vibration in Systems with Time-Varying Resonances," *Proceedings of the 1887 IEEE International Conference on Robotics and Automation*, Raleigh, NC, pp. 1690-1695.

9. Singer, N.C. and Seering, W.P., "Preshaping Command Inputs to Reduce System Vibration," AIM No. 1027, The Artificial Intelligence Laboratory, Massachusetts Institute of Technology, January, 1988.

10. Singer, N.C. and Seering, W.P., "Design and Comparison of Command Shaping Methods for Controlling Residual Vibration," *Proceedings of the 1989 IEEE International Conference on Robotics and Automation*, Scottsdale, AZ, pp.888-893.

11. Singer, N.C., *Residual Vibration Reduction in Computer Controlled Machines*, Ph.D. Thesis, Massachusetts Institute of Technology, February, 1989.

12. Yuan, B.S., *Adaptive Strategies for Controls of Flexible Arms*, Ph.D. Thesis, Georgia Institute of Technology, April, 1989.

13. Magee, D.P., *Dynamic Control Modification Techniques in Teleoperation of a Flexible Manipulator*, Masters Thesis, Georgia Institute of Technology, November, 1991.

Experimental Verification of Modified Command Shaping Using a Flexible Manipulator

David P. Magee and Wayne J. Book

George W. Woodruff School of Mechanical Engineering, Georgia Institute of Technology, Atlanta, GA

ABSTRACT

A brief discussion introduces the original input shaping method applied to a system with varying parameters. A change in parameters causes a vibration in the system and a modified command shaping technique is created to eliminate this unwanted motion. Using a two degree of freedom (DOF), flexible manipulator, experiments are conducted by varying perturbations to input trajectories to compare the modified method to a previously used adaptive proportional plus derivative (P.D.) control method. The control scheme that produces the smaller magnitude of resonant vibration at the first natural frequency of the robot is considered the more effective control method.

KEY WORDS: command shaping, flexible manipulator, adaptive P.D. control, vibration reduction

INTRODUCTION

With an increase in environmental concern, the interest in long-reach, flexible manipulators has grown significantly in the last few years. The long, slender links of the flexible manipulator have a desirable strength-to-weight ratio and are cheaper to build than their rigid link counterparts. However, the inherent flexibility of the links generates a residual vibration that makes end-point positioning of the tip difficult. In most robotic applications, accurate end-point positioning is desired. Therefore, a method to eliminate the residual vibration of a flexible manipulator is the main focus of this paper.

The reduction of residual vibration in a manipulator is not a new idea. Many active and passive control schemes exist that were designed to eliminate vibration. One of the most rudimentary passive approaches is to move the robot to a desired location and wait for the vibration to subside. For example, the Space Shuttle Remote Manipulator system is very inefficient in task completion time. Other passive methods include the addition of a second mass which behaves like a vibration absorber or the application of a visco-elastic material that absorbs vibrational kinetic energy [1].

The active control strategies include spectral methods where the command signal is modified so that vibration is not induced into the system. Meckl and Seering [2] developed a direct relationship between the frequency spectrum of the input signal and the resulting vibration. By reducing the spectral magnitude of the input at the resonances of the system, the residual vibration is eliminated. Their work showed promising results if the change in system resonant frequency was less than about 10%. Later, they extended their work to develop a set of force profiles that will accelerate a system to a given velocity level with minimum residual vibration [3].

Another way of reducing the spectral magnitude at the resonances is to add zeros to the system function at the locations of the poles. Singer and Seering [4,5] developed an input shaping technique that alters commanded inputs using the characteristics of the system. Each sample of the input is transformed into a new set of impulses that do not excite the system resonances. However, this method cannot accommodate systems that contain time varying parameters so a modified shaping method is developed. To fully appreciate the modified command shaping technique, Singer and Seering's input shaping method will now be presented.

INPUT SHAPING METHOD

The dynamic equations of a manipulator become quite complex when the flexibility of the links is considered. To greatly simplify the problem, the dynamics of the manipulator are assumed to be a linear combination of flexible and rigid body motion. The flexible motion is often called the residual vibration of the system where as the desired trajectory is the rigid body motion. The original input shaping method developed by Singer and Seering models the residual vibration of a system as a simple, second-order system. The impulse response of a linear, time-invariant, underdamped second-order system can be written as

Presented at 1st International Conference on Motion and Vibration Control, Sept 7-11, 1992, Yokohama, Japan.

$$x(t) = \frac{A\omega_n e^{-\zeta\omega_n(t-t_0)}}{\sqrt{1-\zeta^2}} \sin\left(\omega_n\sqrt{1-\zeta^2}(t-t_0)\right) \quad (1)$$

where A is the amplitude of the impulse, ω_n is the natural frequency of the system, ζ is the damping ratio, t is the time and t_0 is the time when the impulse occurs. Since the input shaping technique generates a new set of impulses, the method will be explained using a set of two impulses. The second-order system response to a set of two input impulses is

$$x(t) = B_1\sin(\alpha t + \phi_1) + B_2\sin(\alpha t + \phi_2) \quad (2)$$

where

$$B_i = \frac{A_i\omega_n}{\sqrt{1-\zeta^2}} e^{-\zeta\omega_n(t-t_{0i})} \quad (3) \qquad \alpha = \omega_n\sqrt{1-\zeta^2} \quad (4) \qquad \phi_i = -\omega_n t_{0i}\sqrt{1-\zeta^2} \quad (5)$$

and t_{0i} signifies the time at which the i^{th} impulse occurs. The two impulse input response given in Equation (2) can be simplified to yield

$$x(t) = B_{amp}\sin(\alpha t + \psi) \quad (6)$$

where

$$B_{amp} = \sqrt{[B_1\cos(\phi_1) + B_2\cos(\phi_2)]^2 + [B_1\sin(\phi_1) + B_2\sin(\phi_2)]^2} \quad (7) \qquad \psi = \tan^{-1}\left(\frac{B_1\sin(\phi_1) + B_2\sin(\phi_2)}{B_1\cos(\phi_1) + B_2\cos(\phi_2)}\right). \quad (8)$$

Since the purpose of the input shaping method is to eliminate vibration, the amplitude of vibration, Equation (7), must equal zero after the second impulse occurs. This only occurs if the squared terms are independently zero since the sine and cosine functions are orthogonal. The resulting set of equations are

$$B_1\cos(\phi_1) + B_2\cos(\phi_2) = 0 \quad (9) \qquad B_1\sin(\phi_1) + B_2\sin(\phi_2) = 0 \quad (10)$$

which can be solved for the two impulse amplitudes and the times at which they occur. Since Equations (9) and (10) are transcendental, an infinite number of solutions exist. Therefore, only the solution that yields the shortest time duration between impulses with positive amplitudes is chosen. The resulting solution is

$$A_1 = \frac{1}{1+M} \quad (11) \qquad t_{01} = 0 \quad (12)$$

$$A_2 = \frac{M}{1+M} \quad (13) \qquad t_{02} = \frac{\pi}{\omega_n\sqrt{1-\zeta^2}} \quad (14) \qquad M = e^{-\frac{\zeta\pi}{\sqrt{1-\zeta^2}}}. \quad (15)$$

From Equation (14), notice that the second impulse occurs at one-half the damped oscillation period of the system. Intuitively, the second impulse creates a vibration that attempts to cancel the vibration generated by the first impulse. The amount of remaining residual vibration is defined by a vibration error expression. A detailed discussion of the vibration error can be found in previous work by Magee [6].

TIME VARYING PARAMETERS

Although the original input shaping technique eliminates residual vibration, the method does not address the issue of varying system parameters. For many flexible robot systems, the natural frequency and damping ratio are functions of position. As the robot moves through joint space the parameters change. The effect of time varying parameters on the input shaping method will now be discussed and then a modified command shaping technique

is presented.

To develop this new technique, the implementation of the original input shaping algorithm to a discrete-time system is presented. In the general case, for each sample of the input, the input shaping method creates a set of N impulses. From Equation (14), the output impulses are equally spaced in time with a continuous-time period, denoted *delT*, of

$$delT = \frac{\pi}{\omega_n \sqrt{1-\zeta^2}} \tag{16}$$

which is a function of both the natural frequency, ω_n, and damping ratio, ζ. To utilize this time period information in a discrete-time control system, the continuous-time data must be represented in discrete-time. From discrete-time signal processing, a continuous-time signal, $x(t)$, is represented mathematically as a sequence of numbers, $x[n]$, where n is strictly an integer. To transform the continuous-time period *delT* into a discrete-time period, *deln*, the sampling rate of the discrete-time system, f_s , is used. The equation to perform this transformation is

$$deln = int(delT * f_s) \tag{17}$$

where the *int* function truncates its argument to an integer.

For Singer's original input shaping method, the discrete-time period, *deln*, never changes because the system parameters are assumed constant. When the input shaping method is applied to a system with time varying parameters, the continuous-time period, *delT*, becomes time varying as well. A significant change in *delT* will result in a change in the discrete-time period, *deln*, which produces a vibration in the system. This induced vibration will be verified later in this paper.

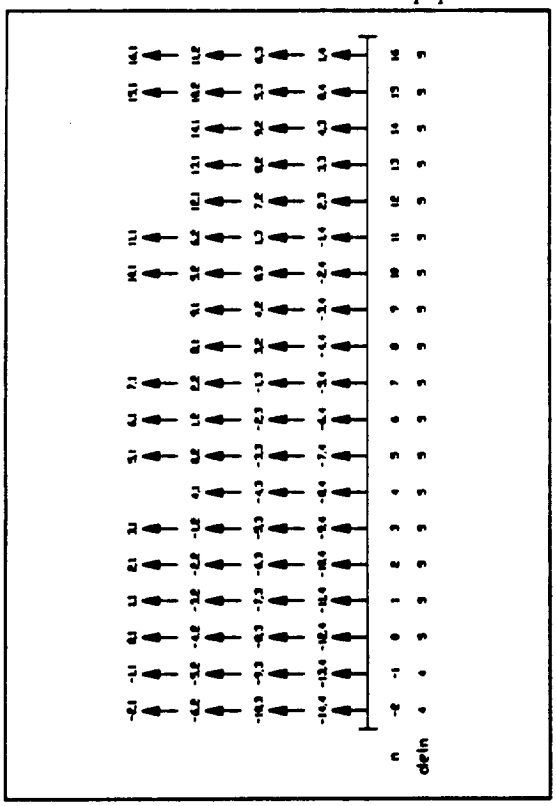

Fig.1 Steady-State Output for an Increase in Discrete-Time Period Using Input Shaping

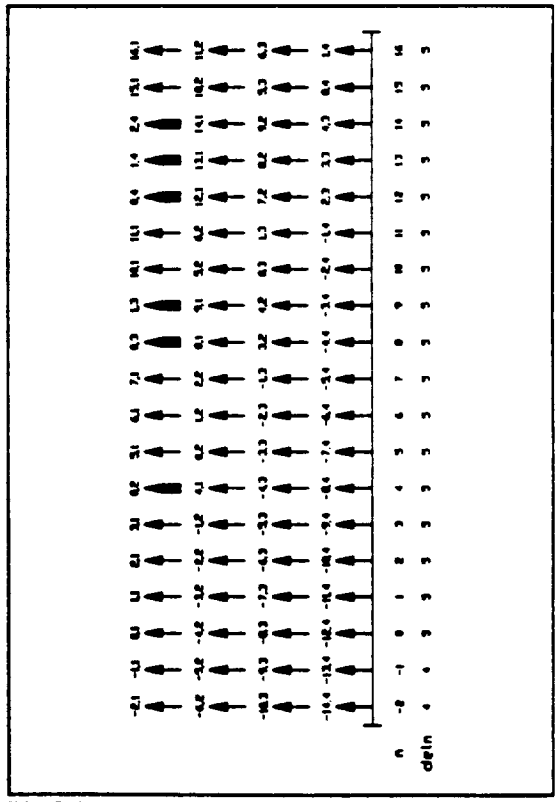

Fig.2 Steady-State Output for an Increase in Discrete-Time Period Using MCS

The effect of time varying parameters on the input shaping method can also be demonstrated graphically. Consider the input shaping method that produces four new impulses for each sample of the desired input. Now assume that a change in system configuration alters the value of the discrete-time period. Figure 1 shows the steady-state impulse output for a change in discrete-time period, *deln*, from four to five. Each output impulse is designated $\{a,b\}$ where a indicates the discrete-time location of the input sample responsible for the four output impulses and b indexes the four resulting output impulses. After examining Fig.1, it is obvious that the change in

deln has caused gaps in the output for discrete values of n. At $n=4$, for example, only three impulses contribute to the overall output. To make matters worse, this lack of impulses is repeated five more times at a discrete-time period near the system's natural period. This phenomenon induces a vibration into the system that is caused solely by the application of the input shaping method to a system with time varying parameters. The vibration is also present when the value of *deln* decreases. In this case, an excess of impulses is created which are spaced at integer multiples of the system's natural period [7].

To eliminate the induced vibration, a modified command shaping method is proposed to make the impulse output more uniform when a change in *deln* is encountered. To compensate for the change in discrete-time period, extra impulses are added for an increase in *deln* and impulses are removed for a decrease in *deln*. The choice of which impulses are affected is based on the number of output impulses from the shaping algorithm and the old and new values of the discrete-time period.

MODIFIED COMMAND SHAPING

The previous section showed that Singer's original input shaping method produces gaps in the output for systems with time varying parameters. To smooth the output, a modified command shaping method is developed. When the discrete-time period increases, designate the discrete-time value as $n=0$. The modified command shaping technique transforms the next N-1 samples of the input, i.e. $0 \leq n \leq N-2$, using both the old and new values of *deln*. Using the new value of *deln*, the input sample is shaped to create N output impulses that are added to the steady-state output at their respective discrete-time values. Using the old value of *deln*, the same input sample is also shaped to create N output impulses. However, only the last $N-(n+1)$ output impulses are added to the steady-state output at their respective discrete-time values. For discrete-time values of $n \geq N-1$, each sample of the input is shaped normally using the new value of *deln* to generate the N output impulses.

The steady-state impulse output for an increase in discrete-time period using the modified shaping method is shown in Fig.2. The darkened impulses emphasize the impulses added by the modified shaping method. Comparing this output to Fig.1, it is apparent that the new impulse profile is much smoother than the original input shaping method.

The modified command shaping method also works for a decrease in the discrete-time period. Designating the discrete-time value as $n=0$, the input sample is shaped only once using the new value of *deln* to produce N output impulses. Instead of adding all of the output impulses, only the first $(n+1)$ output impulses are added to the steady-state output at their respective discrete-time values. By manipulating the steady-state output in this manner, the extra impulses that are added for the increase in discrete-time period are the same indexed impulses that are removed when *deln* decreases.

COMPARISON OF THE SHAPING METHODS

By shaping the error term in an adaptive feedback control system developed by Yuan [8], the two shaping methods are now compared using a precomputed desired trajectory. The principal trajectory consists of a circle in cartesian space that is three feet in diameter with a period of nine seconds. The circle was positioned in the workspace of the manipulator so that a change in the discrete-time period would occur. To measure the vibration of the system, an accelerometer was mounted at the tip of the manipulator. A signal analyzer records the time response of the accelerometer and computes the frequency response of the data. To ensure reliable averaging of the data, the manipulator is commanded to follow the desired trajectory eight times.

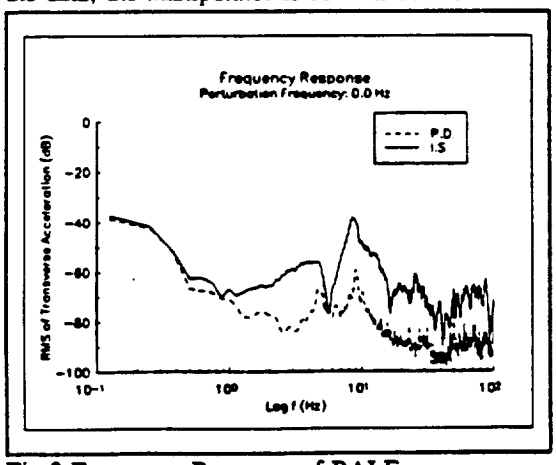

Fig.3 Frequency Response of RALF
P.D. vs. Input Shaping

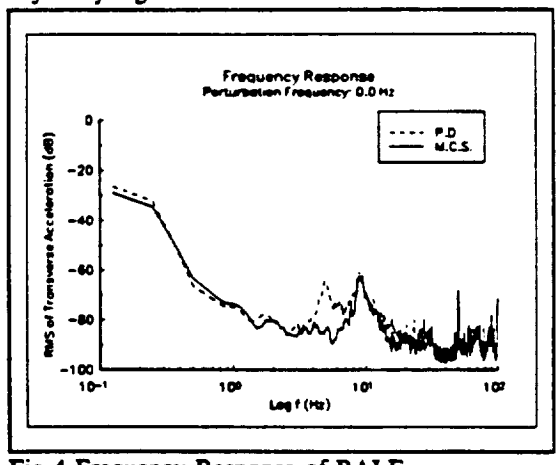

Fig.4 Frequency Response of RALF
P.D. vs. Modified Command Shaping

The first comparison is between Singer's input shaping method and Yuan's adaptive P.D. control structure. Figure 3 presents the spectral comparison for these two techniques. Notice that the magnitude of the frequency response for the input shaping method is much greater than for the adaptive P.D. routine alone. At the frequency range that the input shaping method is designed to control (3.7-5.5 Hz), the frequency response is 12 dB larger. This is due to a change in discrete-time period which induces vibration at the system resonance. It is also worth noting that the second resonance of RALF occurs near 10 Hz and is also very evident in Fig.3.

The next comparison is between the modified command shaping method and Yuan's adaptive P.D. control algorithm. The spectral comparison for these two methods is shown in Fig.4. From this figure, the modified method has reduced the magnitude of the resonant vibration at the first frequency range by almost 20 dB. Therefore, the modified method has reduced the vibration by nearly 32 dB over the input shaping method. Again, this increase in performance is due to the inability of the input shaping method to accommodate a change in discrete-time period.

DESIRED TRAJECTORIES WITH PERTURBATIONS

Now that the modified shaping method controls systems with varying parameters, the circle trajectory used previously will be altered. A sinusoidal perturbation with variable frequency is added to the radius parameter of the circle to simulate the frequency components of possible telerobotic inputs. The frequency response of the modified method will be compared to that of the adaptive P.D. routine to determine the better control scheme.

The first trajectory, shown in Fig.5, contains a 1 Hz sine wave with an amplitude of 1.5" riding on the radial component of the circle. Notice that this trajectory has nine "bumps" around the circle since the period is nine seconds. The frequency response comparison for this trajectory is shown in Fig.6. Since the command shaping technique was not designed to eliminate 1 Hz vibration, the two control schemes show comparable results for this frequency range. However, the modified method reduces the magnitude of vibration by 18 dB at the first natural frequency value of 4.8 Hz. This results in a vibration that is 1.6% of the amplitude of the original adaptive P.D. vibration at this particular frequency.

The second trajectory contains a 4.8 Hz sine wave added to the principal circle and is designed to excite the first natural frequency of RALF. Figure 7 displays the frequency response comparison for this trajectory. The difference in magnitude is 32 dB at the first natural frequency which corresponds to 0.06% of the adaptive P.D. vibration at this frequency value.

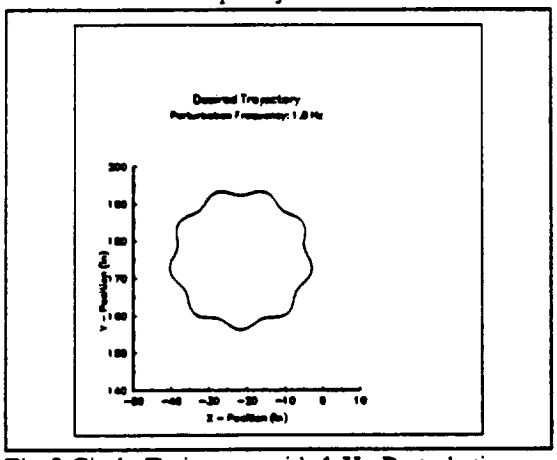

Fig.5 Circle Trajectory with 1 Hz Perturbation

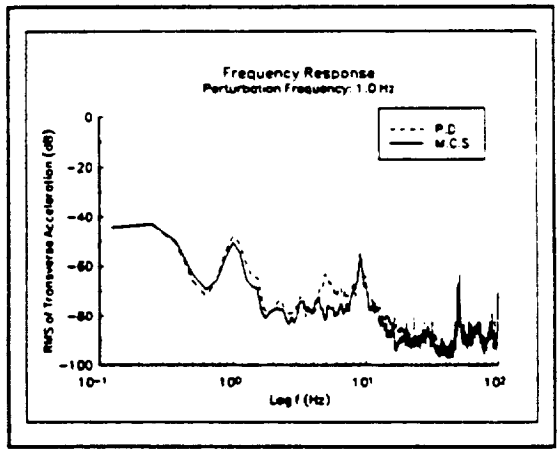

Fig.6 Frequency Response of RALF
P.D. vs. Modified Command Shaping
1 Hz Perturbation

The last circular trajectory was designed to have a perturbation resonance above the first natural frequency of RALF. For this trajectory, a 10 Hz sine wave is added to the principal circle. Figure 8 shows a reduction in magnitude of the frequency response at the 4.8 Hz frequency location of 9 dB. This results in a vibration that is 12.6% of the amplitude of the original adaptive P.D. vibration for this particular frequency. For all three test cases, the modified shaping method was able to reduce vibration at the first natural frequency of the manipulator.

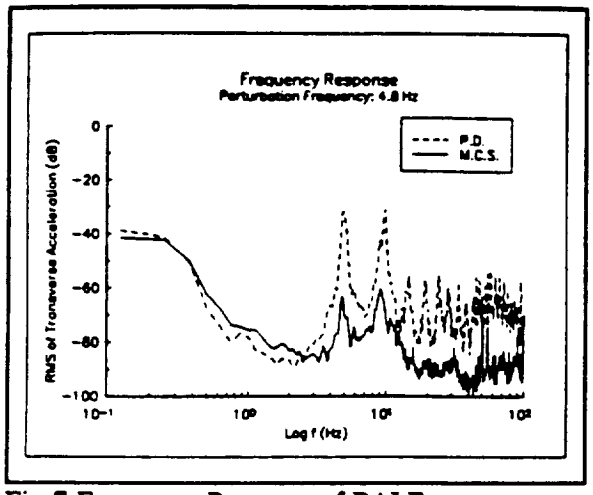

Fig.7 Frequency Response of RALF
P.D. vs. Modified Command Shaping
4.8 Hz Perturbation

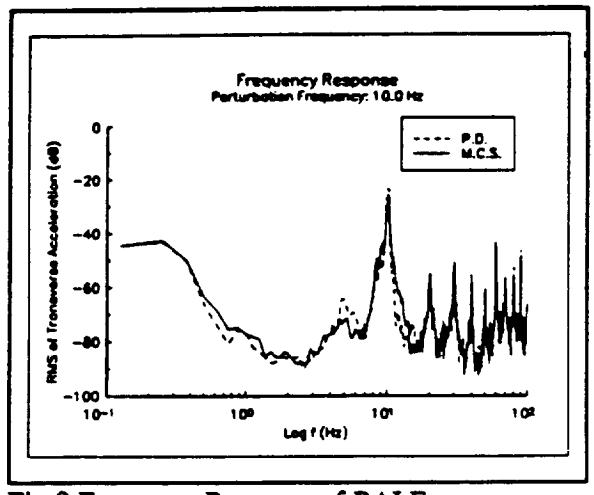

Fig.8 Frequency Response of RALF
P.D. vs. Modified Command Shaping
10 Hz Perturbation

CONCLUSION

The original input shaping method developed by Singer and Seering was presented and was shown to induce vibration in a manipulator that contains time varying parameters. To eliminate the induced vibration, a modified command shaping technique was developed. The modified method was able to reduce vibration at the first natural frequency of the system for input trajectories containing different sinusoidal perturbations. Thus, the modified shaping method offers considerable vibration reduction for inputs with multiple frequency components.

REFERENCES

1. Alberts, T.E., Hastings, G.G., Book, W.J. and Dickerson, S.L., "Experiments in Optimal Control of a Flexible Arm with Passive Damping," *Fifth VPI&SU/AIAA Symposium on Dynamics and Control of Large Structures*, Blacksburg, VA, 1985.

2. Meckl, P.H. and Seering, W.P., "Reducing Residual Vibration in Systems with Time-Varying Resonances," *Proceedings of the 1987 IEEE International Conference on Robotics and Automation*, Raleigh, NC, pp.1690-1695.

3. Meckl, P.H. and Seering, W.P., "Controlling Velocity-Limited Systems to Reduce Residual Vibration," *Proceedings of the 1988 IEEE International Conference on Robotics and Automation*, Philadelphia, PA, pp.1428-1433.

4. Singer, N.C. and Seering, W.P., "Preshaping Command Inputs to Reduce System Vibration," AIM No. 1027, The Artificial Intelligence Laboratory, Massachusetts Institute of Technology, January, 1988.

5. Singer, N.C., *Residual Vibration Reduction in Computer Controlled Machines*, Ph.D. Thesis, Massachusetts Institute of Technology, February, 1989.

6. Magee, D.P., *Dynamic Control Modification Techniques in Teleoperation of a Flexible Manipulator*, Masters Thesis, Georgia Institute of Technology, November, 1991.

7. Magee, D.P. and Book, W.J., "The Application of Input Shaping to a System with Varying Parameters," to appear in 1992 JAPAN/USA Symposium on Flexible Automation.

8. Yuan, B.S., *Adaptive Strategies for Controls of Flexible Arms*, Ph.D. Thesis, Georgia Institute of Technology, April, 1989.